Identifying and quantifying erosion beneath the deposits of long-runout turbidity currents along their pathway

J.E. Hunt[1]*

[1]*National Oceanography Centre, European Way, Southampton SO143ZH, UK*

*Corresponding author: james.hunt@noc.ac.uk

Keywords: turbidites, erosion, Itrax, coccolith biostratigraphy

Abstract

Variations between the geochemical compositions, coccolith species compositions and the physical properties of turbidite muds and their underlying hemipelagites can be used to understand the erosive nature of sediment gravity flows. Large-volume submarine landslides on the NW Moroccan continental margin produce long-runout turbidity currents capable of traversing hundreds-to-thousands of kilometres across the adjacent Moroccan Turbidite System (MTS). These turbidity currents are responsible for turbidites that are among the largest-volume, most aerially extensive, and longest-runout deposits recorded. These resulting turbidite beds can be correlated over distances of greater than 1,800 km across the full 250,000 km^2 area of the MTS. Due to the ability to trace these individual flow deposits throughout the MTS large-volume beds A5, A7, A11, A12 and A15 can be shown to be erosive upon debouching Agadir Canyon, whilst smaller-volume flows were not erosive. These aforementioned large-volume flows have been capable of eroding up to 15 km^3 of material in the Canyon mouth, equating to as much as 50% of the later deposit volume. Evidence suggests individual flows erode up to 4.5 m of sediment within scours in the mouth of Agadir Canyon. However, these scours are greater than 8.0 m deep, indicating that several

flows contribute to forming the scours in a series of cut and fill episodes. Several flows, including beds A5, A7, A11 and A12 were also erosive in Agadir Basin up to 210 km from the canyon. The present study indicates that large-volume flows A5, A7 and A12 are also erosive within the channel-lobe transition zone within the proximal Madeira Abyssal Plain after exiting the Madeira Channels, over 800 km from Agadir Canyon. Studying the deposits of these flows and their compositional changes along their entire pathway has provided invaluable information of whether the flows are erosive, where this erosion takes place, and to what extent they erode the seafloor. There are also broader implications towards gaining information about flow processes at the bed interface, calculating basin sediment budgets and better understanding discontinuous stratigraphy in distal turbidite systems

1. Introduction

Submarine landslides and their associated sediment gravity flows are hazards to seafloor infrastructure used for recovering oil and gas, which can be worth tens of millions of dollars (Barley, 1999; Talling *et al.*, 2014). Turbidity currents and debris flows are also capable of breaking seafloor telecommunication cables that carry global data traffic (Piper *et al.*, 1999; Carter *et al.*, 2012; Pope *et al.*, 2017). Erosion by these flows can scour, undermine and destabilise seafloor infrastructure. Ancient deposits of these mass movements represent among the largest marine hydrocarbon reserves (Stow and Mayall, 2000). Erosion by ancient flows can both amalgamate reservoir-quality sand layers or remove them entirely, thus influencing hydrocarbon recovery (Stephen *et al.*, 2001). Resolving the pathways and erosive behaviour of past mass movements will enable better hazard mitigation of modern gravity flows and understanding of potential reservoir connectivity in ancient marine deposits. Without direct monitoring, determining past erosive capabilities can provide insights into the fluid mechanics of these potentially destructive, large-volume and long-runout flows and how they evolve (Talling *et al.*, 2007, 2014; Stevenson *et al.*, 2014b; Talling, 2014). Importantly, resolving the erosivity of past flows can also provide important insights into sediment budgets in marine environments.

The Late Quaternary Moroccan Turbidite System (MTS) is located offshore the Northwest African passive margin and comprises three interconnected deep-water provinces: Agadir Basin, Madeira Abyssal Plain and Seine Abyssal Plain (Figure 1) (Wynn *et al.,* 2000, 2002a). Large-volume (>0.1 km^3), siliciclastic, organic-rich turbidites are sourced from the Moroccan continental slope via Agadir Canyon and deposited throughout these interconnected basins (Pearce and Jarvis, 1992). Individual deposits are correlated between core sites tens-to-hundreds of kilometres apart with high certainty based on chemostratigraphy, biostratigraphy and physical properties of both the turbidites and intervening hemipelagite (Weaver *et al.*, 1992; Wynn *et al.*, 2002a; Hunt *et al.*, 2013a, 2013b). Therefore, this study area represents an excellent opportunity to investigate how individual turbidity currents have flowed over runouts of >1,000 km and areas >200,000 km^2 and interacted with the seafloor (Weaver *et al.*, 1992; Wynn *et al.*, 2002a; Talling *et al.*, 2007; Stevenson *et al.*, 2014b).

The principal aim of this contribution is to determine where continental slope-derived turbidity currents are erosive in the Moroccan Turbidite System outside the Agadir Canyon during the last 250 ka, where this erosion took place and how much erosion took place. Calculating the volume of sediment added by erosion to the flows will provide an estimation of erosive budgets as flows exit Agadir Canyon and enable better estimation of the flow volume prior to this erosion, which may better reflect the size of the original failure. This research is timely as it is reliant on the robust correlation of single beds throughout the turbidite system, which has only been made possible recently (Hunt *et al.*, 2013a, 2013b). Direct monitoring has shown that small-volume submarine flows are capable of eroding and immediately depositing sediment causing migrating bedforms (Hughes-Clark, 2012, 2014). However, little is known about erosion beneath large-volume flows, such as those monitored in Congo Canyon that may last for prolonged periods of time (Andrieux *et al.*, 2013), especially the basal flow conditions and their interaction with the sea floor.

This study will first validate correlating individual turbidites between the Agadir Canyon, Agadir Basin and Madeira Abyssal Plain. Then it will investigate individual flow deposits to determine if their original flows have been erosive, where this erosion took place and how much sediment was eroded in terms of volume and erosive depth. To do this, three complimentary and novel chemostratigraphy, biostratigraphy and physical property methodologies were used to uniquely identify and quantify erosion beneath submarine flows.

2. Geological Setting

Agadir Basin is a ~100 km-wide elongate deep-water basin (~4400 m) fed primarily by Agadir Canyon on the Moroccan continental margin (Figure 1) (Wynn *et al.,* 2002a). It comprises two sub-basins separated by a low-gradient ramp (Talling *et al.,* 2007; Wynn *et al.,* 2010). The largest flows are able to exit Agadir Canyon, transit Agadir Basin, enter the Madeira Channel System, and run out onto the more distal Madeira Abyssal Plain (Masson, 1994; Wynn *et al.,* 2002a; Hunt *et al*., 2013b; Stevenson *et al.,* 2013).

The Agadir Basin turbidite stratigraphy in isolation represents a sequence of interbedded siliciclastic, volcaniclastic, and calciclastic beds ranging in volume from 1 to 30 km^3 (Wynn et al., 2002a; Frenz *et al.,* 2009; Hunt *et al.,* 2013a). The Madeira Abyssal Plain also has a well-developed turbidite stratigraphy with numerous beds exceeding 200 km^3 (Weaver and Kuijpers, 1983; Weaver *et al.*, 1992; Hunt *et al.*, 2013a, 2013b, 2014; Clare *et al.*, 2014). The turbidite stratigraphy of Agadir Basin, Madeira Abyssal Plain and adjacent Seine Abyssal Plain can be correlated over the last 150 ka, with individual events extending over >200,000 km^2 across all three basins (Wynn *et al.*, 2002a; Hunt *et al.*, 2013a). The most recent siliciclastic beds A5, A7 and A12 in Agadir Basin have been shown to correlate to beds Md, Me and Mf in the Madeira Abyssal Plain, respectively (Wynn *et al.*, 2002a).

3. Methodology and Data

Core JC27/13 from Agadir Canyon represents a site up-stream to erosive scouring in the canyon mouth, providing a new record of flows that reach the end of the canyon pathway (Figure 1). Core D13073 on the northern slope of Agadir Basin comprises a record of flows exiting the canyon in the last 600 ka (Hunt *et al.*, 2013a). Agadir Basin cores were recovered from the low-gradient ramp on the eastern basin margin (including CD166/48), the flat upper sub-basin (including CD166/57), the low-gradient ramp between upper and lower sub-basins (including CD166/31), and the flat lower sub-basin (including CD166/12) (Figure 1). A final core (D11813) is also used from the channel-lobe transition zone between the Madeira Channel System and the Madeira Abyssal Plain (Figure 1).

3.1 Visual and sedimentological logging

Selected piston cores from Agadir Basin, Madeira Abyssal Plain and adjacent slopes were visually logged (Figure 1). Sediment facies, colour, grain-size, sedimentary structures and sand mineralogy were all documented.

3.2 Itrax μXRF of hemipelagite

High-resolution down-core micro-XRF Ca variability of the hemipelagite using the *Itrax* core scanner is used to support correlation of turbidites between core sites by their position within an established record of temporal Ca variations linked to sealevel changes (Hunt *et al*., 2013a). This has previously been demonstrated in Agadir Basin cores CD166/48, CD166/57, CD166/31, CD166/12 and D13073 (Hunt *et al*., 2013a). Turbidites recovered from Agadir Canyon site JC27/13 are correlated to those in Agadir Basin and to those in the 600 ka record from D13073 (Hunt *et al*., 2013a). New down-core hemipelagite Itrax-Ca data from D11813 in the Madeira Abyssal Plain is used to correlate beds into the turbidite record at CD166/12 in Agadir Basin.

3.3 Coccolith biostratigraphy

Coccolith biostratigraphy has been previously used to both correlate and date turbidites in Agadir Basin and the Madeira Abyssal Plain (Weaver *et al*., 1992; Wynn *et al*., 2002a; Hunt *et al*., 2013a, 2013b). Coccolith biostratigraphy was completed on core JC27/13 in Agadir Canyon for this study, in order to provide accurate and robust datum horizons to correlate beds between Agadir canyon, Agadir Basin and Madeira Abyssal Plain.

The last occurrence of *Helicosphaera inversa* is at 140 ka (Hine, 1990), while the last occurrence of *Gephyrocapsa ericsonii* is at 15 ka (Biekart, 1989). The relative abundances of *Pseudoemiliania lacunosa*, *Gephyrocapsa caribbeanica*, *Gephyrocapsa aperta*, *Gephyrocapsa mullerae* and *Emiliania huxleyi* are used to constrain acme zones that correlate to oxygen-isotope stage (OIS) boundaries (Weaver and Kuijpers, 1983; Weaver, 1994). Indeed, noteworthy changes in these relative abundances include: dominance in *G. caribbeanica* below OIS 7 with a marked decrease from the OIS8-OIS7 boundary (290 ka), onset in dominance of *G. aperta* during OIS7 and OIS6, onset in dominance of *G. mullerae* at

~120 ka within OIS5, and onset in the dominance of *E. huxleyi* from OIS5 onwards (71 ka) (Weaver and Kuijpers, 1983).

Samples were taken every 5 cm through the hemipelagite in JC27/13, at 1-3 cm intervals at hemipelagite lithological boundaries, and above and below every turbidite. Hemipelagite was identified by: lack of sedimentary structures, randomly dispersed foraminifera, variable but commonly abundant bioturbation, fine-grained texture, and a typically brownish or greyish colouration (with tone depending on calcium carbonate content). Pinhead-sized samples were diluted and smeared onto SEM semi-conductor stubs using acetone (Hunt *et al.*, 2013a, 2013b). Each sample had >300 coccolith specimens counted to assess species abundances using the *Hitachi TM1000* bench-top SEM (Appendix 3). Some glacial-aged clays (OIS4) lacked sufficient coccolith numbers and/or specimens due to the effects of dissolution. Precision was found to be within 2-4% standard deviation upon repeat sampling.

Coccolith biostratigraphy for D11813 in the Madeira Abyssal Plain was taken from Hunt *et al.* (2013b). Coccolith biostratigraphy for Agadir Basin cores CD166/12, CD166/31, CD166/57, CD166/48 and D13073 were taken from Hunt *et al.* (2013a). The biostratigraphy was combined with new down-core Itrax micro-XRF compositional data of hemipelagites to correlate cores throughout the system.

3.3 Physical properties logging to detect erosion

Physical properties including p-wave velocity, gamma ray density, magnetic susceptibility and sediment lightness (L* in CIELAB space) were measured using the *GeoTek Multisensor core logger* (*MSCL*) at 0.5 cm intervals down core. Data pertaining to turbidites were removed from the records, which enabled comparison of the physical properties of the hemipelagite immediately above and below the turbidite. This allows identification of offsets in the record caused by erosive removal of otherwise continuous hemipelagic sedimentation. Although excursions or offsets in all four data are preferred to demonstrate erosion, excursions or offsets in at least two of the properties are required to determine erosion and to negate erroneous data artificially creating an excursion, and incorrectly inferring erosion. Geochemical and coccolith compositions of turbidite mudcaps were only completed on select cores, whilst physical property analyses were completed on all cores collected on the D118, CD166 and JC027 research cruises to Agadir Basin. These mudcaps represent fine-grained sediment deposited from the suspension of turbidity currents under low energy equating to the Bouma T_e division. This method provides a greater sample resolution in Agadir Basin to identify the presence of erosion, but not how much has taken place.

3.4 Itrax μXRF compositions of turbidite mudcaps

Geochemical compositions of turbidite mudcaps at JC27/13 are compared to those of the same turbidites in core CD166/48 to assess erosion of flows exiting the canyon (Figure 1). Comparison of mudcap compositions of the same turbidite along the Agadir pathway (cores CD166/48, /57, /31 and /12) will also enable identification of whether the flows have been erosive in Agadir Basin, specifically where along the pathway erosion has occurred and potentially to what extent. Data is only taken from below the oxidation fronts as oxidation fronts result in remobilisation and re-precipitation of mobile elements, thus changing the composition of the oxidised sediment from the original. Comparison of mudcap compositions of the same flow between core CD166/12 in the distal Agadir Basin and D11813 in the Madeira Abyssal Plain will enable assessment of whether flows were erosive upon exiting the Madeira Channels (Figure 1); on the assumption that the flows were bypassing within the Madeira Channel System itself and not erosive (Stevenson *et al*., 2013).

Cores are analysed using the Itrax micro-XRF core scanner; whereby split core sections of each core are progressively moved past a 3 kW Mo-tube X-ray source and XRF Si-drift chamber detector (Croudace *et al.,* 2006). The instrument operated at 60 kV and 45 mA, with a dwell time of 800 ms, and a down-core resolution of 500 µm (Hunt *et al*., 2015a, 2015b). Comparison of mudcap compositions of similar grain-size distributions reduces effects of sample geometry (Hunt *et al*., 2015a, 2015b). Compositions are only taken from beneath the oxidation fronts in these deposits, as elements are preferentially mobilised above these fronts, altering the compositions (Wilson et al. 1986; Jarvis & Higgs, 1987). Attempts thus far to convert XRF core scanner outputs to elemental concentrations have been moderately successful (Weltje and Tjallingii, 2008; Hunt *et al*., 2015a, 2015b; MacLachlan *et al.*, 2015). Element ratios will instead be used in this study, because they reduce the impact of sample geometry and unit-sum constraint and dilution (Weltje and Tjallingii, 2008). Numerous studies have advocated using element ratios, and here selected ratios are used according to Croudace *et al.* (2006) and Rothwell *et al.* (2006), and are summarised in table 1. Use of ratios also removes the affects of carbonate content (Pearce and Jarvis, 1992; Hunt *et al*., 2015a).

In the absence of reliable Al data, due to its low atomic weight and subsequent attenuation of K-shell X-rays, immobile Ti was substituted to normalise the data. Due to the often greater reliability of Ti data, it is used instead Rb, which would otherwise have better reflected Al composition.

3.5 Itrax µXRF comparisons of turbidite mudcap and hemipelagite compositions

Itrax turbidite mudcap geochemical compositions within Agadir Basin will also be compared to the composition of hemipelagite sediments immediately below each bed. This will enable assessment of the extent to which hemipelagite below each turbidite has been eroded, mixed, and incorporated into the overriding flow. For example, turbidite A3 mudcap composition is compared to the hemipelagite below it separating turbidites A3 and A5 termed HP3-5.

3.6 Grain Size Analysis

Down-core grain size analyses were firstly undertaken to evaluate control of grain-size on geochemistry, whereby grain-size exerted no discernable control on geochemical composition (Hunt *et al.*, 2015a; Appendix 1). Grain-size samples from turbidite mudcaps were used to verify consistent grain-size distributions analysed by Itrax, where mudcap grain-size varied by less that 5% (Hunt *et al.*, 2015a; Appendix 2). Grain size-samples were also taken from the turbidite bases to provide information on the maximum grain sizes of sediment transported in each flow. One cm^3 samples were dispersed in 0.05% sodium hexametaphosphate solution, shaken for 12 hours, and analysed using the *Malvern Mastersizer 2000*. Aliquots are sub-sampled by an autosampler whilst the sediment is being agitated and all sediment in suspension. Three sample aliquots were each measured three times over 60 sec. Measurements of multiple aliquots and repeat samples showed precisions to within 3% of the mean average value, whilst measures of *Malvern* reference materials showed accuracies to within 2% of the certificate mean average, d10 and d90 values.

3.7 Calculation of depth of erosion using coccoliths

Five samples were also taken through each turbidite mudcap from JC27/13, CD166/48, CD166/57, CD166/31, CD166/12 and D11813. The changes in relative coccolith species abundances allowed the depth of erosion beneath each flow along the flow pathway to be calculated, and from this estimates of volume added by erosion. The depth of erosion was calculated using a method developed by Weaver (1994). This involves first taking the relative abundance of coccoliths species at the site upstream from erosion and then the site of interest. Simulated coccolith mixtures from progressively older oxygen isotope stages are added to the coccolith compositions of turbidite upstream of erosion until it matches the composition of the same turbidite in the basin. The high resolution biostratigraphic information from Hunt *et al*. (2013a, 2013b) enabled addition of relative coccolith abundances at 2-to-10 ka time intervals, rather than using average compositions over whole marine oxygen isotope stages as per Weaver (1994). This method provides an age of hemipelagite added to the flow by erosion that is converted to a depth of erosion by applying known hemipelagite accumulation rates from Hunt *et al*. (2013a, 2013b), depths of erosion are resolved to conservatively within 5-10 cm accuracies. The volume of sediment added by erosion to result in the changes to the coccolith relative abundance is calculated using a mass balance to within ±10 km^3, given the large initial volume of the turbidity currents. Erosion is restricted to removal of fine-grained hemipelagite in many cases, and so the mud volumes are used in the calculation of erosion budgets, whilst the sand volume is kept constant reflecting its original volume input from the slide.

4. Results

4.1 Correlation and dating of beds between Agadir Canyon, Agadir Basin and Madeira Abyssal Plain

The chrono-stratigraphy for JC27/13 is based upon the position of turbidite beds in relation to the hemipelagite Itrax-CaO micro-XRF record (chemostratigraphy), hemipelagite lithostratigraphy and coccolith biostratigraphy (Figure 2):

- The last occurrence of *G. ericsonii* at 15 ka at 7 cm hemipelagite depth, last occurrence of *H. inversa* at 140 ka at 110 cm hemipelagite depth, and first occurrence of *E. huxleyi* at 291 ka at 178 cm hemipelagite depth provide datum horizons (Figure 2).
- Coccolith acme zones provide datum horizons defined by decrease in abundance of *G. caribbeanica* at 177 cm depth dated at 290 ka, decrease in abundance of *G. aperta* at 64 cm dated at 120 ka, and the decrease in *G. mullerae* and increase in *E. huxleyi* abundances dated at 71 ka (Figure 2).
- A further set of datums at 48 cm and 18 cm hemipelagite depths concern excursions in *G. mullerae* abundances due to dissolution of finer coccolith shields in association with glacial OIS2 and OIS4 intervals (Figure 2).
- Peaks (generally >35-40 wt% CaO) and troughs (generally <20-30 wt% CaO) within the CaO hemipelagite chemostratigraphy can be correlated to respective peaks and troughs in the Lisiecki and Raymo (2005) global benthic foraminifera $\delta^{18}O$ record. This provides added resolution to dating the turbidites, especially in conjunction with the lithology of the hemipelagite and coccolith biostratigraphy.

Specific beds can be identified by their location within this hemipelagite biostratigraphy and CaO chemostratigraphy, supporting their dating and correlation between the canyon and basin sites (Figures 2 and 3). The turbidite record in JC27/13 is compared to those recovered from the established stratigraphy within the basin and at a site to the north of the canyon (D13073) (Figure 3). This highlights how the beds are correlated with confidence between the basin and the canyon, which commences with a series of marker beds:

- A coarse gravel lag containing abundant pyrite and lithics is located above a red clay (OIS4) dated at ~60 ka using coccolith biostratigraphy; this represents bed A5 (Figure

2). This red clay immediately below the bed represents hemipelagite carbonate depletion associated with OIS4 dissolution (Figures 2 and 3); this is confirmed with the down-core hemipelagite CaO-profile. A hemipelagite sedimentation rate of 1.44 cm/1000 year at JC27/13 also identifies this gravel bed as bed A5 (Figure 2).

- There is a fine pale-grey turbidite mud within the hemipelagite above the A15 turbidite, which represents the bed A14 Icod turbidite marker bed (~165 ka) from the Icod landslide on Tenerife (Figure 2; Hunt *et al.* 2011). This pale-grey, low K/Ti and Fe/Ti, structureless and homogenous mud is located within a low-carbonate red marl identified as OIS6, which is consistent with bed A14 within the basin (Figure 3).

- The next coarsest turbidite in bed A15 (basal grain size >250 µm) at 3.50-3.80 m core depth resides above white interglacial clay. The hemipelagite CaO profile and application of a 1.44 cm/1000 year hemipelagite sedimentation rate dates the event to ~200 ka (Figure 2). This siliciclastic bed A15 in JC27/13 correlates with bed A15 in D13073 in (Figure 3). The glacial red-clay above is the OIS6 clay and the white hemipelagite below is the OIS7 calcareous ooze (Figures 2 and 3).

Coccolith biostratigraphy and the tie-points above support the correlation of the JC27/13 hemipelagite Itrax-CaO micro-XRF down-core record to the Lisiecki and Raymo (2005) global benthic $\delta^{18}O$ record (Figure 2). The relatively low frequency of beds and development of 5-10 cm of hemipelagite between individual beds is a major advantage for correlating turbidites in this system. This enables dating of the turbidites at site JC27/13 to ±5 ka and importantly allows confident correlation of individual turbidites from the canyon to basin (summarised in table 2).

Previous studies date and correlate turbidites across the Madeira Abyssal Plain (Weaver *et al.*, 1992; Hunt *et al.*, 2013a, 2013b), and correlate them into the stratigraphy of Agadir Basin

(Wynn *et al.*, 2002a; Hunt *et al.*, 2013a, 2013b). This study validates the correlation of siliciclastic beds *Mc*, *Md*, *Me*, *Me1* and *Mf* in the Madeira Abyssal Plain (represented in D11813) with beds A3, A5, A7, A11 and A12 in Agadir Basin, respectively, using both coccolith biostratigraphy and hemipelagite Itrax-CaO micro-XRF profiles (Figure 2).

4.2 Erosion between Agadir Canyon and Agadir Basin

Evidence of erosion from Itrax mudcap geochemical compositions

Beds A3 and A13 do not vary in geochemical composition between the Agadir canyon mouth (JC27/13) and basin plain (Figure 4A and 4F), whilst bed A5 varies significantly between those sites (Figure 4B). Beds A7, A11 and A12 also vary significantly, with a shift and offset of the canyon composition compared to the basin (Figure 4C, 4D and 4E). Finally, bed A15 shows significant difference between Agadir Canyon and the margin of Agadir Basin, where piston coring penetrates deep enough to recover the bed (Figure 4F). Thus beds A3 and A13 are inferred to be non-erosive, whilst beds A5, A7, A11, A12 and A15 are inferred to have been erosive.

The compositions of the smaller beds, found only in the proximal region of the upper sub-basin (e.g. CD166-48), were also compared to equivalent deposits in the Agadir Canyon (JC27/13). Beds A1.6, A3.1, A7.1 and A10.1 in both Agadir Basin and Agadir Canyon were broadly similar, with overlapping compositions (Figure 5). The smaller beds older than bed A13 could not be analysed in Agadir Basin due to lack of core penetration to those depths. However, these beds are recovered in core D13073 on the basin margin. Beds A17, A21.1, A21.2 and A21.3 have similar geochemical compositions in the Agadir Canyon and the basin margin (Figure 5). Thus these smaller-volume flows are inferred to have been non-erosive upon exiting Agadir Canyon.

Evidence of erosion from turbidite coccolith assemblages

Beds A3 and A13 show <5% differences in relative abundances of individual coccolith species between the canyon and the basin sites (Figures 6 and 7; Table 3). Beds A5, A7, A11, A12 and A15 show considerable compositional variation between the canyon and the basin (Figures 6 and 7; Table 3). These particular beds show a 50% reduction in the abundance of *P. lacunosa* and between 5 and 20% increases in *G. aperta* and *G. caribbeanica* abundances (Figures 6 and 7). This indicates that the larger-volume A7, A11, A12 and A15 flows have been erosive upon exiting Agadir Canyon, adding younger sediment to their flows.

To cause the compositional variation in bed A5 required erosion to depths equating to 200 ka, representing erosion of 2.0-2.2 m of sediment when using the 1.44 cm/1000 year sedimentation rate at JC27/13 (Figures 6 and 8). To generate the compositional change in bed A7, bed A11 and bed A12 at the canyon mouth requires erosion to depths corresponding to hemipelagites of 160 ka, ~300 ka and no older than 450 ka age, respectively (Figures 6 and 8). When using the 1.44 cm/1000 year sedimentation rate at JC27/13, this equates to maximum depths of erosion of 1.4-1.5 m, 2.2-2.5 m and 4.2-4.7 m, respectively. Bed A15 shows compositional variation indicating that there has been erosion on an order of <1 m. These variations are summarised in table 3.

Within the smaller beds, e.g. A1.6, A3.1, A7.1, A10.1, and those older than bed A15, e.g. A17, A23.1, A23.2, A23.3, the coccolith compositions in Agadir Canyon at JC27/13 are compared to those at D13073 on the basin margin (Figure 8). Cores in the basin lack the depth of penetration to recover the olderbeds. These particular beds do not show any variation between the canyon and basin margin, indicating little-or-no erosion (Figure 8).

4.3 Erosion within Agadir Basin

Evidence of erosion from sediment core physical properties

The previous section used geochemical and coccolith compositional changes in the turbidites between Agadir Canyon and the basin to investigate whether erosion had taken place in the canyon mouth and estimate depths of erosion. Addition of seafloor sediment to the flows by erosion would alter their composition accordingly. In this section geochemical and coccolith compositions are also analysed in four sediment cores 70-80 km apart within Agadir Basin (Figure 1). However, core scans of physical properties (i.e. P-wave velocity, gamma ray density, magnetic susceptibility and lightness of colour as L*) have also been collected from all cores in Agadir Basin, providing a means to determine whether erosion has taken place across the entirety of the basin and at core sites at closer intervals of 10-30 km.

Small-volume beds A3 and A13 show no evidence of erosion throughout Agadir Basin. Furthermore, small-volume beds A1.4, A1.6, A3.1, A3.2, A3.3, A7.1, A7.2 and A10.1 also all show no evidence of erosive removal of hemipelagite sediment in the uppermost Agadir Basin before they terminate. Large-volume siliclastic flows exiting Agadir Canyon are non-erosive in the distal regions of Agadir Basin over 140-150 km from Agadir Canyon, with the exception of bed A5. Hemipelagite physical property records show no offsets caused by erosive removal of seafloor sediment by flows in the lower sub-basin between CD166/31 and CD166/24 (Figures 9 and 10). However, there is erosion beneath the large-volume flows detected by offsets in down-core hemipelagite physical properties in the upper sub-basin (Figures 9 and 10).

There is erosion beneath bed A7 in the upper sub-basin within a 30 km-wide corridor, but evidence of erosion disappears beyond CD166/34, ~140 km from Agadir Canyon (Figures 9 and 10). Bed A11 was also erosive in the upper sub-basin, but only as far as CD166/57, located 110 km from Agadir Canyon, but this occurs over a broader 40 km-wide corridor (Figures 9 and 10). Within cores proximal to Agadir Canyon recovery often halted in the sand of bed A12, thus analysing pre- and post-event hemipelagite compositions could not completed for this bed proximal to Agadir Canyon. However, there is evidence of erosion at site CD166/51 and CD166/52, inferring that erosion did occur within a corridor between 20 and 70 km wide (Figure 10). Evidence indicates that bed A12 was at least not erosive at CD166/34, 140 km from Agadir Canyon (Figures 9 and 10).

Bed A5 shows evidence of erosion throughout the central region of the upper sub-basin and the upper portions of the lower sub-basin. Not only did this flow erode hemipelagite but was also capable of eroding previously deposited beds, e.g. bed A7 is eroded out at CD166/51 (Figure 9). Evidence of erosion beneath bed A5 is however restricted to a narrow 20-25 km-wide corridor through the centre of the basin (Figures 9 and 10). Evidence of erosion disappears beyond site CD166/30, located 185 km from Agadir Canyon.

Evidence of erosion from Itrax mudcap geochemical compositions

Beds A3 and A13 show no variation in mudcap composition within Agadir Basin (Figure 4A, 4C and 4F). Beds A7, A11 and A12 show minor geochemical compositional variations between the proximal site CD166/48 and more distal sites in Agadir Basin (Figure 4D and

4E). The geochemical composition of bed A7 in the Again Basin diverges from that in the canyon mouth. At site CD166/57, Bed A7 shows greater Fe/Ti and the greatest divergence from the original composition compared either with more proximal CD166/48 or more distal sites, implicating erosion between CD166/48 and CD166/57, and potentially as far as CD166/31 in order to change the composition. Beds A11 and A12 also show greater elevated Fe/Ti at CD166/57, implicating erosion at this site and the more proximal CD166/48 site. However, throughout the remainder of the basin the large-volume turbidites, except bed A5, have similar mudcap geochemical compositions from site-to-site (Figure 4B). This likely indicates that little-or-no erosion takes place beneath these flows beyond the proximal regions of the upper sub-basin. The bed A5 mudcap geochemical composition has a narrower compositional range distally in the lower sub-basin and a different broader compositional range in the upper sub-basin (Figure 4B). This indicates that bed A5 is erosive through much of the upper basin, creating a broader mixed composition, and became only marginally erosive through the lower sub-basin, such that Fe/Ti and K/Ti are elevated at CD166/12 relative to CD166/31.

To further examine whether individual turbidites have significantly eroded underlying hemipelagite on their passage to the western Agadir Basin, the geochemical compositions of the turbidite mudcaps were compared with those of hemipelagic sediments directly underlying the turbidite. The mudcap compositions of beds A3 and A13 from more distal sites in Agadir Basin do not overlap with the underlying hemipelagite, showing no erosive incorporation of hemipelagite into their flows. Although the composition of beds A7, A11 and A12 in Agadir Basin show different compositions to the hemipelagite beneath them, there are overlaps between compositions from sites CD166/48 and CD166/57 and the underlying hemipelagite (Figure 11). This implies that there has been erosion and mixing of hemipelagite sediment whilst flows transit through the upper Agadir Basin. The mudcap composition for bed A5 shows overlap with the underlying hemipelagite, partially at distal sites CD166/31 and CD166/12, but most significantly at proximal sites CD166/48 and CD166/57 (Figure 11B). This suggests that within the basin the flow has been erosive and incorporated hemipelagite sediment within the upper basin and partly within the lower basin (Figure 11B).

Evidence of erosion from turbidite coccolith assemblages

Beds A3 and A13 show no changes in coccolith assemblage through Agadir Basin, as <3% differences are within analytical error (Figure 6). Evidence from the physical properties logs and mudcap geochemical compositions indicates that beds A7, A11 and A12 were erosive in the proximal upper sub-basin. Changes in coccolith compositions support this, whereby beds A7, A11 and A12 show minor increases in *G. aperta* in the proximal Agadir Basin between sites CD166/48 and CD166/57 (Figure 6). Hemipelagite immediately below these beds is rich in *G. aperta*, thus erosion could only be 20-40 cm, as greater erosion would further alter either the abundance of *G. mullerae* or *G. caribbeanica* significantly. Deeper erosion would also result in erosive removal of beds lower in the stratigraphy for which there is no evidence.

Bed A5 is erosive through the proximal Agadir Basin with an increase in *G. aperta* (14%) and decreases in *E. huxleyi* and *G. caribbeanica* at CD166/48. This would require erosion to hemipelagite of 110 to 125 ka age, implicating a depth of erosion of 60-90 cm. Erosion continues beyond CD166/48 with a further increase in *G. mullerae* (12%) and *E. huxleyi* (10%) at CD166/57 (Figure 6; Table 3). This requires a depth of erosion to sediment 70-110 ka old, equating to a maximum erosive depth of 40-60 cm. In addition, samples were taken from mud-chips of hemipelagite sediment within the coarse-sand base of bed A5 at site CD166/57 (Figure 8). These mud-chips represent the hemipelagite sediment eroded by the flow travelling through the upper sub-basin of Agadir Basin. The lithology of these mudchips includes brown glacial clay hemipelagite, pale brown glacial clay hemipelagite, and white interglacial ooze. The coccolith assemblages of these hemipelagite mud-chips indicate that these are OIS4 and upper OIS5 age (Figure 8). This supports the inferred depth of erosion, based on the change in coccolith assemblages in the proximal Agadir Basin (Figure 8). The increase in *G. mullerae* in the lower sub-basin indicates that again sediment of 70-110 ka age was added, implicating erosion of as little as 10 cm but as much as 60 cm (Figure 8).

4.4 Erosion in the proximal Madeira Abyssal Plain

Evidence of erosion from Itrax mudcap geochemical compositions

Bed A13 does not have an equivalent in the Madeira Abyssal Plain. Beds Mc and Me1 in the Madeira Abyssal Plain are equivalent to beds A3 and A11 in Agadir Basin, and have mudcap compositions that are similar to the distal Agadir Basin site CD166/12 (Figures 4A and 9D). Furthermore, neither bed Mc nor Me1 compositions overlap with those of the underlying hemipelagite (Figures 8A and 8D). This suggests that neither flow was erosive upon exiting the Madeira Channel System and entering the Madeira Abyssal Plain.

Conversely, although beds Md, Me and Mf (bed A5, A7 and A12 equivalents) show overlap with the hemipelagite compositions at CD166/12 within Agadir Basin, there is also overlap with the composition of the underlying hemipelagite (Figure 11). This suggests erosive addition and mixing of hemipelagite material into these flows as they exited the Madeira Channel System.

Evidence of erosion from turbidite coccolith assemblages

Beds Mc (bed A3) and Me1 (bed A11) do not show variations in the coccolith assemblages between CD166/12 and D11813 (adjacent core 86PC17 was used for bed Mc as it is not present in D11813) within the channel-lobe region of the Madeira Abyssal Plain (Figure 6). Bed Mf (bed A12) shows a minor increase in *G. mullerae* and more than 5% increase *G. aperta* abundances, while *G. caribbeanica* show a minor reduction, but *P. lacunosa* are completely depleted. To satisfy these changes in coccolith composition erosion of sediment as old as 165 ka took place. Beyond this would increase *G. aperta* too much and alter mudcap geochemical compositions considerably as erosion would start to incorporate sediment from volcaniclastic bed Mg (bed A14, Icod landslide bed from Tenerife, Hunt *et al.*, 2011) (Figure 6). Madeira Abyssal Plain sedimentation rates are ~0.5 cm/1000 year (Hunt *et al.*, 2013b). This results in the bed Mf (bed A12) flow eroding up to 20 cm of sediment upon exiting the Madeira Channel System (Table 4).

Beds A5 and A7 also show variations in coccolith assemblages. Increases in *E. huxleyi* and *G. mullerae* abundances within bed Md (bed A5) require erosion to sediment 90-110 ka old, equating to 15-25 cm erosion (Figures 6 and 9, Table 4). Bed Me (bed A7) requires erosion to sediment no older than 175 ka, equating removal of as much as 40 cm in the channel-lobe transition zone (Table 4).

4.5 Estimating erosive budgets

To calculate the erosive budgets of these flows, the calculations have to be completed in reverse, thus working backwards from distal to proximal, from Madeira Abyssal Plain to Agadir Basin, to Agadir Canyon. They are calculated using mass balances combining information from the known depths of erosion, known depositional volumes and the compositional changes caused by erosion.

Erosion between Madeira Channels and Abyssal Plain

Table 4 shows the volume of sand and mud reaching the Madeira Abyssal Plain in each flow. Sand is considered to comprise the original flow material not significantly contributed to by erosion of hemipelagite, as this eroded sediment comprises mostly fine-grained clays and coccoliths, with minimal siliciclastic minerals and foraminifera. From the Madeira Channels into the Madeira Abyssal Plain bed A3 (bed Mc) and bed A11 (bed Me1) have not been erosive (Figures 4A, 4D, 6, 9A and 9D). Bed A5 is erosive and the flow added 15% mud volume to produce the required change in coccolith composition. Thus 5.1 km^3 has been eroded not just in the channel-lobe transition area, but over an area of ~25,500 km^2 (Figures 4B, 6, 8B and 9, Table 4).

Bed A7 requires 15% of the mud volume to originate from erosion (Figures 4C, 6, 8C and 9, Table 4). Therefore bed A7 has eroded ~15.5 km^3 by removing up to 40 cm of hemipelagite over an area of 38,000 km^2 (Table 4). Finally, bed A12 involves addition of 10% volume to the flow of sediment from no more than 20 cm below the seafloor (Figures 4E, 6, 8E and 9, Table 4). Bed Mf has a volume of 190 km^3 in the Madeira Abyssal Plain (Weaver, 1994), thus to alter the composition on this scale erosion occurs over an area half the size of the Madeira Abyssal Plain.

Erosion within Agadir Basin pathway

The flow volumes transiting Agadir Basin represent a combination of the original volume, material eroded from the canyon and material eroded from Agadir Basin. Firstly, new volumes are calculated by removing the volumes of erosive material added between Agadir Basin and Madeira Abyssal Plain (Table 4).

Beds A3 and A13 show minimal coccolith assemblage or geochemical changes along the Agadir Basin pathway, indicating little-to-no erosion beneath these flows (Figure 6). The changes to the composition of bed A7 in the proximal upper sub-basin shows that erosion likely occurred to between 10 and 40 cm depths. This is supported by a lack of removal of lower stratigraphic units by erosion beneath bed A7. Less than 3% of the flow volume of bed A7 is gained by erosive addition of sediment in Agadir Basin, which equates to an erosive volume of 2.6 km^3 over 6,500 km^2. This compares favourably with evidence of erosion from physical properties logs of Agadir Basin cores that indicate a conservative area of 3,900 km^2 over which erosion occurs beneath bed A7 (Figures 9 and 10)

Beds A11 and A12 show minimal changes in mudcap coccolith assemblages and geochemical compositions beyond the proximal areas of the upper sub-basin (Figures 4 and 6). To maintain the observed coccolith compositions and no evidence that turbidites lower in the stratigraphic sequence have been erosively removed by either bed A11 or A12, erosive depths of 10 and 40 cm in the proximal upper sub-basin are prescribed, respectively (Figure 4 and 6). The change in composition of beds A11 and A12 requires addition of less than 5% volume in Agadir Basin. For bed A11 this was achieved by erosion of 10 cm over 3,900 km^2, which compares well to conservative estimates of erosion beneath bed A11 over an area of 4,400 km^2 (Figures 9 and 10). For bed A12 around 5% of its flow volume is gained by erosion within Agadir Basin, this would require erosion to 40 cm over an area of 12,000 km^2. From the limited constraints on the area of erosion beneath bed A12 from the physical properties logs would be between 2,800 km^2 and 9,800 km^2, which supports the larger estimate of the erosion area (Figures 9 and 10).

Bed A5 shows a more complex erosional history. The distal Agadir Basin sites record the flow composition after erosion upon debouching the canyon. Sites CD166/48 and CD166/57 in the proximal Agadir Basin show extensive local erosion (Figures 4B, 6, 9 and 11B). Bed A5 gained 30% of its mud volume by erosion of hemipelagite to a depth up to 90 cm (Figures 4B, 6, 9 and 11B; Table 4). This results in the flow removing roughly 8.65 km^3 over an area of 9,600 km^2 (Table 4). Further erosion is also seen beneath bed A5 in the lower sub-basin, although erosion this far from Agadir Canyon is likely less than 20 cm (Figures 4B, 6, 9 and 11B; Table 4). Physical properties logs of sediments cores indicate that erosion is restricted to roughly 5,000 km^2, which would imply that the maximum erosion depth may be greater than 90 cm proximally or that erosion has occurred over a much larger area not detected and constrained in the down-core physical properties logs.

Erosion exiting Agadir Canyon

The flow volumes exiting Agadir Canyon represent the original flow volume and material eroded from the canyon mouth. Thus new volumes are calculated by removing the known volumes of erosive material after the flows leave the canyon (Table 4). Beds A3 and A13 had no sediment added between the canyon and basin by erosion. To produce the basin composition of coccoliths in bed A5 requires addition of up to 50% of the flow volume in hemipelagite material (Table 4). This means that bed A5 removed up to 15 km^3 from the Agadir Canyon mouth by removing up to 2.0-2.5 m over 7,500 km^2. Bed A7 also required an addition of 15 km^3, which represents an addition of 15% of the flow volume by erosion from removal of 1.4-1.5 m over a ~700 km^2 area (Table 4). Bed A11 has involved addition of up to 5 km^3 by erosion of up to 2.5 m over 1,900 km^2 (Table 4). Lastly, bed A12 required addition of 15% of its volume by erosion (equating ~20 km^3) of up to 4.5 m over an area of 4,500 km^2 (Table 4).

5. Discussion

5.1 Erosion in the mouth of Agadir Canyon

There are significant changes in the geochemical and coccolith compositions of the large-volume turbidites (beds A5, A7, A11, A12 and A15) between canyon and basin sites (Figures 4 and 6). These compositional differences reflect erosive addition of carbonate-rich sea floor sediment into the respective turbidity current, which is mixed and later deposited.

This study suggests bed A5 required addition of sediment of 60-250 ka age, equating to a 2.0-2.5 m erosive depth (Figures 4 and 6). This is supported by hiatuses of 130 ka recorded below bed A5 dated at 59 ka in the Agadir Canyon mouth scour field (Macdonald *et al.*, 2011). Bed A7 eroded 0.75-1.0 m, bed A11 eroded 2.2-2.5 m, and finally bed A12 eroded 3.0-4.5 m of sediment in the canyon mouth (Figure 8). These depths of erosion are supported by recognition of a major hiatus to OIS13 in cores from the Agadir Canyon scour field, below 130 ka-age turbidites (equivalent to beds A11 and/or A12) (Macdonald *et al.*, 2011). Therefore the estimates of large-scale erosion required for turbidite compositional changes determined from this study are supported by evidence of erosion beneath beds in the scour field.

MacDonald *et al*. (2011) described scour fields in the Agadir Canyon mouth that are often over 8.0 m deep, and scours in alternate systems up to 20 m deep (Wynn *et al.*, 2002b; MacDonald *et al.*, 2011). These scours are prescribed as being long-lived. This present study identifies that erosion is restricted to beneath individual large-volume flows carrying coarse-sediment and generally only erode 0.75 to 4.5 m, and certainly less than 5.5 m (Figures 4, 6, 8, 9 and 10). This demonstrates that individual scours are generated by numerous cutting and filling events, rather than being generated by a single flow. This repetitive scouring of flows of up to 4.5 m presents a significant hazard to installation of seafloor infrastructure, albeit in more active canyon mouths where such events are more regular than the 10-20 ka recurrence of this system (Hunt *et al.*, 2013a). In ancient systems this level of erosion is more than capable of amalgamating sand beds metres thick or removing large proportions of stratigraphy. Thus this identified erosion presents complications to modelling reservoir connectivity and designing of hydrocarbon recovery.

The flows that have been erosive in the canyon mouth have been the largest-volume events and those carrying the coarsest sediment, including beds A5, A7, A11 and A12. These flows also show evidence of bedforms synonymous with higher basal sediment concentrations and basal reworking of sediment (Sumner *et al.*, 2012). MacDonald *et al.* (2011) highlight that erosional scour may be concentrated at the canyon mouth as flows rapidly expand onto the basin plain. Flow expansion with associated decreasing gradient will allow the flows to potentially move from being supercritical to subcritical. The increase in turbulence at this point may be responsible for the erosion and sediment reworking.

Smaller-volume flows still capable of transiting Agadir Basin, such as beds A3 and A13, have not been erosive between canyon and basin sites (Figures 4 and 6). Furthermore, those flows that have exited Agadir Canyon but not flown across the basin have also been shown to be non-erosive, such as beds A1.4, A1.6, A3.1, A3.2, A3.3, 7.1 and A10.1 (Figures 5 and 7). Therefore, small-volume flows (<2 km^3) are not erosive upon exiting the Agadir Canyon. These low-volume events are dilute flows and never supercritical, thus do not experience the hydraulic jump upon exiting Agadir Canyon, and thus are not erosive.

5.2 Implications for erosion of flows within Agadir Basin

Beds A3 and A13 show no discernable erosion beneath their flows in Agadir Basin. There is 10-40 cm of erosion beneath beds A7, A11 and A12, which occurred within the most proximal locations of Agadir Basin (Figures 4, 6, 9, 10 and 11; Table 4). Bed A5 is an exception, showing erosion of up to 90 cm through the centre of the upper sub-basin of Agadir Basin up to 210 km from the canyon and erosion between 10 and 20 cm across the lower sub-basin up to 300 km from the canyon (Figures 4, 6, 8, 9 and 10; Table 4). Whilst these observations provide quantitative support for previously documented erosion beneath bed A5 (Talling *et al.,* 2007; Wynn *et al.,* 2010; Hunt *et al.*, 2013a), this importantly shows that large-volume long-runout flows are capable of erosion in excess of 210 km into the basin, but that this erosion is restricted to the centre of the pathway.

The addition of cohesive fine-grained sediment beneath the flow may have acted to dampen turbulence, especially where there is synchronous decrease in flow velocity as the basin floor gradient decreases (Talling *et al.*, 2007). Dampening of turbulence is best shown within the bed A5 flow with development of the coeval linked-debrite (Talling *et al.*, 2007). The linked-debrite in the upper sub-basin starts to develop between CD166/48 and CD166/57, between which up to 90 cm deep erosion of hemipelagite occurs (e.g. site CD166/51; Talling *et al.*, 2007; Wynn *et al.*, 2010; Hunt *et al.*, 2013a). It is also suggested that the A7, A11 and A12 flows show debritic facies at site CD166/57, potentially indicative of flow transformation from dominantly turbulent to laminar flow (e.g. figure 6 in Hunt *et al.*, 2013a).

Evidence from the Marnosa arenacea Formation and modern outer Mississippi Fan implicate transition from fluid turbulence to laminar flow occurring in the distal regions of flows, perhaps as velocity drops towards its eventual termination, where flows can then no longer sustain sediment in turbulent suspension (Amy *et al.*, 2006; Talling *et al.*, 2010). However, the bed A5 linked debrite occurs within the centre of the flow rather than at the periphery, generating a metre-thick, poorly-sorted, muddy-sand deposit (Talling *et al.*, 2007). Therefore erosion, rather than simply waning turbulent energy (or flow velocity), potentially influences the occurrence and location of flow transformations, and thus has a resulting influence on the geometry and reservoir quality of the deposits.

Previous studies have assumed that no erosion has taken place beneath the flows traversing Agadir Basin (Stevenson *et al.*, 2014b), although calculations imply that erosion should take place proximally. However, by inferring no erosion beneath the flows in the basin it is implied that they must therefore be depositional immediately upon entering the basin (Stevenson *et al.*, 2014b). This present study challenges those assumptions and shows that erosion does take place beneath beds A5, A7, A11 and A12 along the pathway in Agadir Basin, and importantly that this erosion continues for over 210 km after debouching onto the basin floor. This study conversely implies that flows are initially erosive upon entering Agadir Basin and potentially capable of sustaining bypassing conditions before becoming depositional, instead of being immediately depositional. The initial erosive and bypassing flow conditions may help explain the exceptional runout of these large-volume flows into the distal Madeira Abyssal Plain.

Erosion by sheet flows may not only affect the deposits immediately below, but may have influences on development of the entire stratigraphic sequence (Eggenhuisen *et al.*, 2011). Erosion is limited to up to 4.5 m in the Agadir Canyon mouth and up to 90 cm in Agadir Basin. This is comparative to the erosion in the Macigno Formation, which favours the development of thin substrate detachments metres in length (Eggenhuisen *et al.*, 2011). Although such detachments are not reported in the Moroccan Turbidite System, the presence of centimetre-scale rounded hemipelagite clasts in the base of bed A5 at least suggests small blocks of hemipelagite were detached and transported large distances prior to deposition. Centimetre-to-decimetre scale erosion beneath turbidite sheet sandstones of the Oligocene Macigno Formation, Northwest Italy, shows that differential erosion laterally across the sequence can be compensated by overlying deposits, thus affecting the bed geometries of subsequent sediment sequences (Eggenhuisen *et al*., 2011).

Whilst the smaller beds, e.g. A3 and A13, show little-to-no erosion, beds A5, A7, A11 and A12 all show evidence of erosion within Agadir Basin. Furthermore, when this erosion occurs it regularly reaches the OIS5 coccolith-rich carbonate ooze beneath each of these flows, but not beyond (Figure 8). Within Agadir Canyon erosion is restricted to depths of sediment to depths of sediment younger than the OIS13 coccolith-rich carbonate ooze (Figure 8). Furthmore, where erosion does take place it is commonly greater than 10-20 cm. This implies that firstly there is threshold of shear stress that must be exerted on the seabed for erosion to take place, but when this erosion takes places it continues unabated until a material of greater yield strength presents a barrier. This may imply that the coccolith-rich OIS5 and OIS13 carbonate oozes, and less extent OIS9 ooze, gained greater yield strength and shear modulus to resist erosion by the respective flows, compared to normal hemipelagite sedimentation. This has implications as it infers a material properties control on erosion rather than simply reflecting controls from flow properties.

5.3 Erosion of flows exiting Madeira Channels

Previous work has highlighted that negligible-to-no erosion takes place as flows pass through the Madeira Channels and over the Madeira Abyssal Plain (Weaver and Kuijpers, 1983; Weaver *et al.*, 1992; Stevenson *et al.*, 2013). However, the present study highlights that erosion does occur in the channel-lob-transition at the Agadir Canyon mouth and again at the channel-lobe transition upon debouching the Madeira Channels into the Madeira Abyssal Plain. This contribution shows that beds A3 (bed *Mc*) and A11 (bed *Me1*) have not been erosive upon exiting the Madeira Channels (Figures 5 and 9). These flows were fine-grained and low-volume by this point, and were likely low concentration and fine-grained upon reaching the Madeira Channels. Beds A5 (*Md*), A7 (*Me*) A12 (*Mf*) have eroded 4.2-to-15.0 km^3 of hemipelagite upon entering the Madeira Abyssal Plain (Table 4). Considering the restrictions on the depths of erosion and the volumes needed to account for the observed compositional changes, the areas over which the erosion occurs implies erosion extended beyond the channel-lobe transition and across much of the abyssal plain. This contradicts previous studies that imply no erosion occurs beneath flows crossing the Madeira Abyssal Plain (Weaver and Thomson, 1992; Weaver et al., 1992).

This study demonstrates that even at distances greater than 800 km from source erosion still occurs beneath large-volume flows, but that the erosion is concentrated at locations where there is change in the gradient along the pathway. In this instance, the erosion takes place at the channel-lobe transition into the Madeira Abyssal Plain, but not in the channels preceding it. This study highlights the channel-lobe regions of fans as being dynamic areas where flows can still be erosive as well as depositional (Wynn *et al.*, 2002b). Indeed, the presence of grain-size breaks within the deposits of the proximal Madeira Abyssal Plain can attest to flows operating at velocities high enough to bypass fine silt and clay (Stevenson *et al.*, 2014a). In coarser-grained and more proximal locations with higher frequencies of flows this may mean increased hazards levels in modern systems and increased amalgamation of potential reservoir-quality intervals in ancient systems.

Previous work by Weaver and Thomson (1992) suggest that only up to 12% of the total volume of the most recent siliciclastic turbidite in the Madeira Abyssal Plain (bed *Ma*) originates from erosion along the flow pathway. Calculation of basal erosion beneath the volcaniclastic Icod event bed from Tenerife (bed A14 in Agadir Basin) suggests that as little as 3% of the volume may be added by basal erosion (Hunt *et al.*, 2011). This study shows that the large-volume siliciclastic beds A5, A7, A11 and A12 in the Moroccan Turbidite System eroded up to as much as 25 to 50% of their depositional volume. This is two-to-five times as much erosion as is calculated by Weaver and Thomson (1993) and suggests that erosion in the deep sea has a large role in sediment transport budgets across the Earth's surface.

6. Conclusions

This study demonstrates the successful use of novel complimentary methods for determining whether submarine sediment flows have been erosive, and where and to what extent erosion has occurred. The largest-volume beds represent flows that erode up to 4.5 m upon exiting Agadir Canyon, whilst the smaller-volume flows are principally non-erosive. Importantly, this study shows that the scours in the mouth of Agadir Basin result from numerous cut-and-fill events, rather than erosion by a single event. Beds A5, A7, A11 and A12 also remain erosive in the uppermost regions of Agadir Basin, and regions of the lower sub-basin up to 210 km from where they debouch onto the basin floor. Finding that these flows remain erosive over 200 km from Agadir Canyon within the basin, albeit on a scale of tens-of-centimetres, challenges previous perceptions that these flows are non-erosive across deep sea basins and are purely depositional flows. The largest flows including beds A5, A7 and A12 are also erosive later at the channel-lobe transition where the Madeira Channels debouch into the Madeira Abyssal Plain, over 800 km from their original source.

Erosion by these flows is capable of adding up to 50% of the flow volume, which is up to five-times that predicted by previous studies and highlights the importance of erosion beneath submarine flows. With the exception of the large-volume flows, the remaining flows exiting Agadir Canyon in the last 250 ka are non-erosive, therefore still posing the question how such thin sub-critical flows maintain sediment in suspension over such long runouts.

Acknowledgements

The author would like to thank the Marine Geoscience Group at the National Oceanography Centre and the Postgraduate School of the School of Ocean and Earth Science at the University of Southampton for the PhD and staff funding that allowed this work to be completed. The author would also like to acknowledge the support from the NERC Environmental Risks to Infrastructure Innovation Programme grant NE/N012798/1 and the EU FP7-funded ASTARTE (Assessment, Strategy and Risk Reduction for Tsunamis in Europe) Project (grant 603839). The author would also like to thank Professor David Piper, an anonymous reviewer, and editor Professor Gert de Lange for their much appreciated constructive comments that have made this a better article.

References

Andrieux, O., Cooper, C.K., Wood, J., 2013. Turbidity current measurements in the Congo Canyon. In: *Offshore Technology Conference*, Offshore Technology Conference 2013.

Barley, B., 1999. Deepwater problems around the world. *Leading Edge* 18:488–494, http://dx.doi.org/10.1190/1.1438319.

Biekart, J.W., 1989. Coccolithophores in the Upper Quaternary of some southeast Indonesian basins, *Netherlands Journal of Sea Research*, 24 (4), 523-530.

Carter, L., Milliman, J., Talling, P.J., Gavey, R., Wynn, R.B., 2012. Near-synchronous and delayed initiation of long run-out submarine sediment flows from a record-breaking river flood, offshore Taiwan. *Geophysical Research Letters* 39, L12603, http://dx.doi.org/ 10.1029/2012GL051172.

Clare, M.A., Talling, P.J., Challenor, P., Malgesini, G., Hunt, J.E., 2014. Distal turbidite records reveal a common distribution for large (> 0.1 km3) submarine landslide recurrence. *Geology* 42, 263–266, http://dx.doi.org/10.1130/G35160.1.

Croudace, I.W., Rindby, A., Rothwell, G., 2006. ITRAX: description and evaluation of a multi-function X-ray core scanner. In: Rothwell, R.G. (Ed.), *New techniques in sediment core analysis*, Geological Society of London Special Publication 267, 51–63.

Eggenhuisen, J., McCaffrey, W.D., Haughton, P.D., Bulter, R.W., 2010. Shallow erosion beneath turbidity currents and its impact on the architectural development of turbidite sheet systems, *Sedimentology* 58 (4), 936-959.

Frenz, M., Wynn, R.B., Georgiopoulou, A., Bender, V.B., Hough, G., Masson, D.G., Talling, P.J., Cronin, B., 2009. Provenance and pathways of late Quaternary turbidites in the deep-water Agadir Basin, northwest African margin, *International Journal of Earth Sciences* 98 (4), 721-733.

Hine, N., Weaver, P. P. E., 1998. Quaternary. In: Brown, P.R. (Ed.), *Calcareous Nannofossil Biostratigraphy*, Springer Netherlands, pp. 266-283.

Hughes-Clark, J.E., Marques, C.R.V., Pratomo, D. 2014, Imaging active mass-wasting and sediment flows on a fjord delta, Squamish, British Columbia. In: *Submarine Mass Movements and Their Consequences*, Springer International Publishing, pp.249-260.

Hughes-Clark, J.E., Brucker, S., Muggah, J., Hamilton, T., Cartright, D., Church, I., Kuus, P., 2012. Temporal progression and spatial extent of mass wasting events on the Squamish prodelta slope. In: *11th International Symposium on Landslides*, Conference Proceedings, Banff, June 2012.

Hunt, J.E., Wynn, R.B., Masson, D.G., Talling, P.J., Teagle, D.A., 2011. Sedimentological and geochemical evidence for multistage failure of volcanic island landslides: A case study from Icod landslide on north Tenerife, Canary Islands. *Geochemistry Geophysics Geosystems* 12 (12).

Hunt, J.E., Wynn, R.B., Talling, P.J., Masson, D.G., 2013a. Frequency and timing of landslide-triggered turbidity currents within the Agadir Basin, offshore NW Africa: Are there associations with climate change, sea level change and slope sedimentation rates? *Marine Geology* 346, 274-291.

Hunt, J.E., Wynn, R.B., Talling, P.J., Masson, D.G., 2013b. Turbidite record of frequency and source of large volume (> 100 km3) Canary Island landslides in the last 1.5 Ma: Implications for landslide triggers and geohazards. *Geochemistry Geophysics Geosystems* 14 (7), 2100-2123.

Hunt, J.E., Talling, P.J., Clare, M.A., Jarvis, I., Wynn ,R.B., 2014. Long-term (17 Ma) turbidite record of the timing and frequency of large flank collapses of the Canary Islands. *Geochemistry Geophysics Geosystems* 15(8), 3322-3345.

Hunt, J.E., Croudace, I.W., MacLachlan S., 2015a. Use of calibrated ITRAX XRF data in examining turbidite composition and provenance in Agadir Basin, Northwest African passive margin, In: I.W. Croudace and R.G. Rothwell (Eds.), *Micro-XRF Studies of Sediment Cores*, Developments in Paleoenvironmental Research, Springer Netherlands, 127-146.

Hunt, J.E., Wynn, R.W., Croudace I.W., 2015b. Identification, Correlation and Origin of Multistage Landslide Events in Volcaniclastic Turbidites in the Moroccan Turbidite System, In: I.W. Croudace and R.G. Rothwell (Eds.), *Micro-XRF Studies of Sediment Cores*, Developments in Paleoenvironmental Research, Springer Netherlands, 147-172.

Jarvis, I., & Higgs, N., 1987). Trace-element mobility during early diagenesis in distal turbidites: late Quaternary of the Madeira Abyssal Plain, N Atlantic. Geological Society, London, Special Publications, 31(1), 179-214.Lisiecki, L.E., Raymo, M.E., 2005. Correction to “A Pliocene-Pleistocene stack of 57 globally distributed benthic δ18O records”. *Paleoceanography* 20 (2), 179-214.

MacDonald, H.A., Wynn, R.B., Huvenne, V.A.I., Peakall, J., Masson, D.G., Weaver, P.P.E., McPhail, S.D., 2011. New insights into the morphology, fill and remarkable longevity (>0.2 m.y.) of modern deep-water erosional scours along the northeast Atlantic margin. *Geosphere* 7 (4), 845-867.

MacLachlan, S., Hunt, J.E., Croudace, I.W., 2015. The effects of variable water content and grain size on X-ray fluorescence core-scanning measurements in deep sea sediments.

In: I.W. Croudace and R.G. Rothwell (Eds.), *Micro-XRF Studies of Sediment Cores*, Developments in Paleoenvironmental Research, Springer Netherlands, 173-185.

Masson, D.G., 1994. Late Quaternary turbidity current pathways to the Madeira Abyssal Plain and some constraints on turbidity current mechanisms, *Basin Res*earch 6, 17-33.

Pearce, T.J., Jarvis, I., 1992. Composition and provenance of turbidite sands: Late Quaternary: Late Quaternary, Madeira Abyssal Plain. *Marine Geology* 109, 21-51.

Piper, D.J.W., Cochonat, P., Morrison. M., 1999. The sequence of events around the epicentre of the 1929 Grand Banks earthquake: Initiation of debris flows and turbidity currents inferred from sidescan sonar. Sedimentology 46, 79–97, http://dx.doi.org/10.1046/j.1365-3091.1999.00204.x.

Rothwell, R.G., Pearce, T.J. & Weaver, P.P.E. 1992, Late Quaternary evolution of the Madeira Abyssal Plain, Canary Basin, NE Atlantic, *Basin Research* 4, 103-131.

Rothwell, R.G., & Rack, F.R. 2006, New techniques in sediment core analysis: an introduction, In: Rothwell, R.G. (ed) *New Techniques in Sediment Core Analysis*, Geological Society of London, Special Publications, 267, 1-29.

Stephen, K. D., Clark, J. D., Gardiner, A.R., 2001. Outcrop-based stochastic modelling of turbidite amalgamation and its effects on hydrocarbon recovery. *Petroleum Geoscience* 7(2), 163-172.

Stevenson, C.J., Talling, P.J., Wynn, R.B., Masson, D.G., Hunt, J.E., Frenz, M., Akhmetzhanhov, A., & Cronin, B.T. 2013, The flows that left no trace: Very large-volume turbidity currents that bypassed sediment through submarine channels without eroding the sea floor, *Marine Petroleum Geol* 41, 186-205, doi:10.1016/j.marpetgeo.2012.02.008.

Stevenson, C.J., Talling, P.J., Masson, D.G., Sumner, E.J., Frenz, M., Wynn, R.B., 2014a. The spatial and temporal distribution of grain-size breaks in turbidites. *Sedimentology*, 61 (4), 1120-1156.

Stevenson, C.J., Talling, P.J., Sumner, E.J., Masson, D.G., Frenz, M., Wynn, R.B., 2014b. On how thin submarine flows transported large volumes of sand for hundreds of kilometres across a flat basin plain without eroding the seafloor. *Sedimentology* 61 (7), 1982-2019, doi: 10.1111/sed.12125.

Stow, D.A., Mayall, M., 2000. Deep-water sedimentary systems: new models for the 21st century. *Marine and Petroleum Geology* 17 (2), 125-135.

Sumner, E.J., Talling, P.J., Amy, L.A., Wynn, R.B., Stevenson, C.J., Frenz, M., 2012. Facies architecture of individual basin-plain turbidites. *Sedimentology* 59 (6), 1850-1887.

Talling, P. J., 2014. On the triggers, resulting flow types and frequencies of subaqueous sediment density flows in different settings. *Marine Geology* 352, 155-182.

Talling, P.J., Wynn, R.W., Masson, D.G., Frenz, M., Cronin, B.T., Schiebel, R., Akhmetzhanov, A.M., Dallmeier-Tiessen, S., Bennetti, S., Weaver, P.P.E., Georgiopoulou, A., Zühlsdorff, C., & Amy, L.A. 2007, Onset of submarine debris flow deposition far from original giant landslide. *Nature* 450, 541-544.

Talling, P., Clare, M., Urlaub, M., Pope, E., Hunt, J., Watt, S., 2014. Large Submarine Landslides on Continental Slopes: Geohazards, Methane Release, and Climate Change. *Oceanography* 27 (2), 32-45.

Weaver, P.P.E., 1994. Determination of turbidity current erosional characteristics from reworked coccolith assemblages, Canary Basin, north-east Atlantic. *Sedimentology* 41 (5), 1025–1038.

Weaver, P.P.E., Kuijpers, A., 1983. Climatic control of turbidite deposition on the Madeira Abyssal Plain. *Nature* 306, 360–363.

Weaver, P.P.E., Thomson, J., 1993. Calculating erosion by deep-sea turbidity currents during initiation and flow. *Nature* 364, 136–138.

Weaver, P.P.E., Rothwell, R.G., Ebbing, J., Gunn, D., Hunter, P.M., 1992. Correlation, frequency of emplacement and source directions of megaturbidites on the Madeira Abyssal Plain. *Marine Geology* 109, 1–20.

Weltje, G.J., & Tjallingii R. 2008. Calibration of XRF core scanners for quantitative geochemical logging of sediment cores: Theory and application, *Earth Planet. Sci. Lett.*, 274, 423-438.

Wilson, T.R.S., Thomson, J., Hydes, D.J., Colley, S., Culkin, F. and Sørensen, J., 1986. Oxidation fronts in pelagic sediments: Diagenetic formation of metal-rich layers. Science, 232(4753), pp.972-975.Wynn, R.B., Masson, D.G., Stow, D.A.V., Weaver, P.P.E., 2000. The northwest African slope apron: a modern analogue for deep-water systems with complex seafloor topography. *Mar. Pet. Geol.* 17, 253–265.

Wynn, R.B.,Weaver, P.P.E., Stow, D.A.V., Masson, D.G., 2002a. Turbidite depositional architecture across three interconnected deep-water basins on the northwest African margin. *Sedimentology* 49, 1441–1462.

Wynn, R.B., Kenyon, N.H., Masson, D.G., Stow, D.A.V., Weaver, P.P.E., 2002b. Characterisation and recognition of deep-water channel-lobe transition zones, *AAPG Bulletin* 86 (8), 1441-1462.

Wynn, R.B., Talling, P.J., Masson, D.G., Stevenson, C.J., Cronin, B.T., & Le Bas, T.P. 2010, Investigating the timing, processes and deposits of one of the World's largest submarine gravity flows: The 'Bed 5 Event' off Northwest Africa, In: Mosher, D.C., Moscardelli, L., Baxter, C.D.P., Urgeles, R., Shipp, R.C., Chaytor, J.D., Lee H.J. (eds), Submarine Mass Movements and Their Consequences, Advances in Natural and Technological Hazards Research, 28, iii, pp. 463-474, DOI: 10.1007/978-90-481-3071-9_38.

Figures

Figure 1. Map of the Moroccan Turbidite System showing the core locations (yellow circles) and their relationship to the pathway for flows exiting Agadir Canyon. Detailed contour map of Agadir Basin provided in supplementary materials (Appendix 4).

Figure 2. Core panel for JC27/13 (location Figure 1) and the 0-325 ka record of turbidites exiting the Agadir canyon. Magnetic susceptibility profile highlights the location of most turbidites as a proxy for grain-size. Turbidites are removed from the hemipelagic CaO profile, with the locations marked by a black line. Coccolith biostratigraphy is presented as relative species abundances and last and first occurrences. These datums and the turbidites are then projected onto the stacked Lisiecki and Raymo (2005) benthic δ18O record tied to the CaO profile. Dating ties are red lines, while black circles (peaks) and black squares (troughs) are correlated from the hemipelagite CaO profile to the Lisiecki and Raymo (2005) benthic δ18O record.

Figure 3. Hemipelagite ITRAX CaO and coccolith biostratigraphy showing the correlation of turbidites within Agadir Canyon (JC27/13) to those on basin margin adjacent to Agadir Canyon (D13073), in Agadir Basin (CD166/12, CD166/31, CD166/57 and CD166/48), and in the Madeira Abyssal Plain (D11813).

Figure 4. Comparison of the geochemical composition (K/Ti vs Fe/Ti) for unoxidised large-volume turbidite mudcaps in Agadir Canyon (JC27/13), Agadir Basin (CD166/12, CD166/31, CD166/57 and CD166/48), and Madeira Abyssal Plain (D11813). A) Bed A3, B) Bed A5, C) Bed A7, D) Bed A11, E) Bed A12, and F) Bed A13.

Figure 5. Comparison of the geochemical composition (K/Ti vs Fe/Ti) for unoxidised small volume turbidite mudcaps in Agadir Canyon (JC27/13) and Agadir Basin (CD166/48 for beds A1.6, A3.1, A7.1, A10.1 and D13073 for beds A15, A17, A23.1, A23.2 and A23.3). A) Bed A1.6, B) Bed 3.1, C) Bed A7.1, D) Bed A10.1, E) Bed A15, F) Bed A17, G) Bed A23.1, H) Bed A23.2, and I) Bed A23.3.

Figure 6. Coccolith assemblages in the turbidite mudcaps from Agadir Canyon (JC27/13), Agadir Basin sites (CD166/48, CD166/57, CD166/31 and CD166/12), and Madeira Abyssal Plain (D11813).

Figure 7. Coccolith assemblages in the turbidite mudcaps of lower-volume and short runout turbidites from Agadir Canyon (JC27/13) and the northern margin of Agadir Basin (D13073).

Figure 8. Coccolith assemblages of mud-clasts of hemipelagite sediment in the base of bed A5. These are compared against an idealised temporal record of hemipelagite coccolith compositions, the stratigraphic position from which these mud-clasts originate is shown. Maximum depths of erosion of the individual beds along the flow pathway are shown.

Figure 9. Core panel showing physical property logs for cores along a transect through the centre of Agadir Basin from Agadir Canyon to the Madeira Channels. Panels show p-wave

velocity (red), gammar ray density (dark green), magnetic susceptibility (blue) and sediment lightness in L* greyscale (black). The turbidites are removed from the data and replaced by a coloured block denoting their type (siliciclastic, volcaniclastic, and calciclastic). The data above and below each turbidite is tied together with a dashed line. Where erosion has occurred the data above and below the turbidite will not tie and will be offset, where this occurs in more than two datasets a black transparent box is placed. Bed A2 is a volcaniclastic turbidite showing minor erosion in Agadir Basin but is not part of this study. Beds A5, A7, A11 and A12 all show erosion at different points in the basin.

Figure 10. Erosion maps of Agadir Basin for individual sediment flows. Each of the siliciclastic flows that transit Agadir Basin is plotted. The presence of erosion is determined from offsets in the physical properties logs of all the cores recovered from Agadir Basin, examples in figure 9. Question marks are placed where the turbidite was not penetrated, crosses are placed where the turbidite was not deposited at the core site, white circles denote no erosion, red circles denote erosion and yellow circles denote likely erosion suggested by either changes in geochemical or coccolith compositions but not detected in the physical properties logs.

Figure 11. Comparison of unoxidised turbidite mudcaps in Agadir Basin (CD166/12) to the hemipelagic sediment interval immediately below. Focus is on CD166/12 data, but data also shown from alternative sites in Agadir Basin to assess where erosion into hemipelagite takes place (grey symbols in legend). Also data of mudcap composition is provided from the Maderia Abyssal Plain mudcaps. Hemipelagite nomenclature HP #-# indicates the hemipelagite between two designated turbidites. A) Bed A3, B) Bed A5, C) Bed A7, D) Bed A11, E) Bed A12, and F) Bed A13.

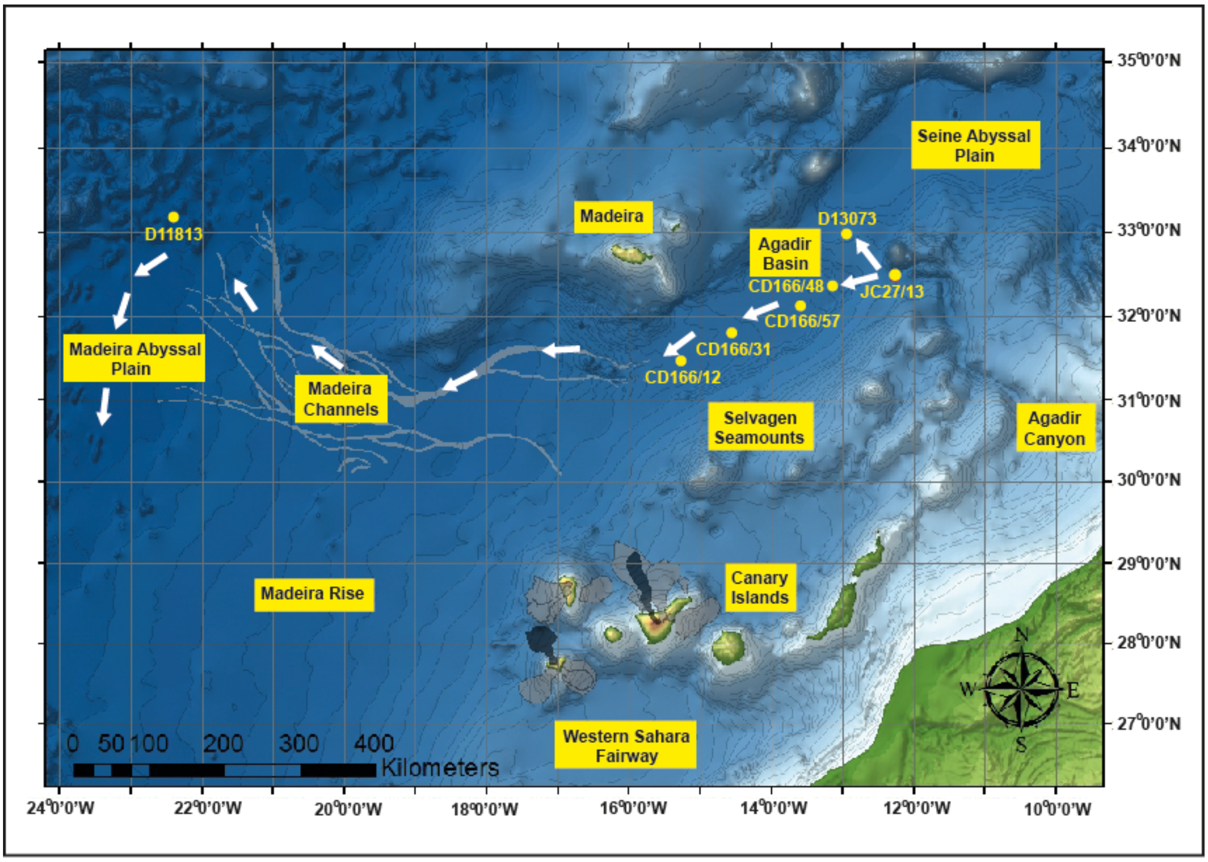
Seine Abyssal Plain
Madeira
D13073
Agadir Basin
D11813
CD166/48
JC27/13
CD166/57
CD166/31
CD166/12
Madeira Abyssal Plain
Madeira Channels
Selvagen Seamounts
Agadir Canyon
Canary Islands
Madeira Rise
Western Sahara Fairway
0 50 100 200 300 400
Kilometers
N
W
E
S
35°0'0"N
34°0'0"N
33°0'0"N
32°0'0"N
31°0'0"N
30°0'0"N
29°0'0"N
28°0'0"N
27°0'0"N
24°0'0"W
22°0'0"W
20°0'0"W
18°0'0"W
16°0'0"W
14°0'0"W
12°0'0"W
10°0'0"W

Figure 1

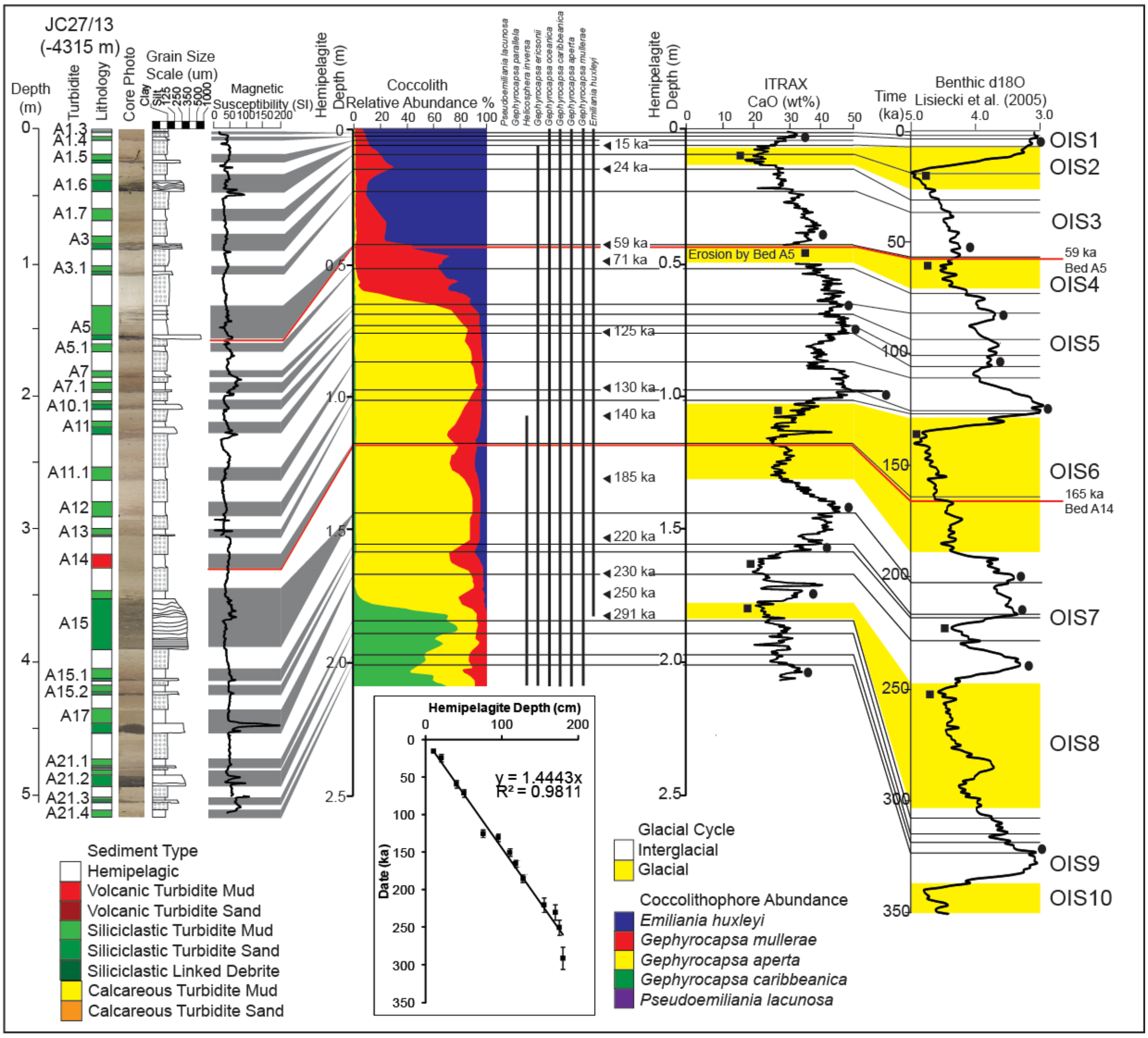

960

961 Figure 2

962

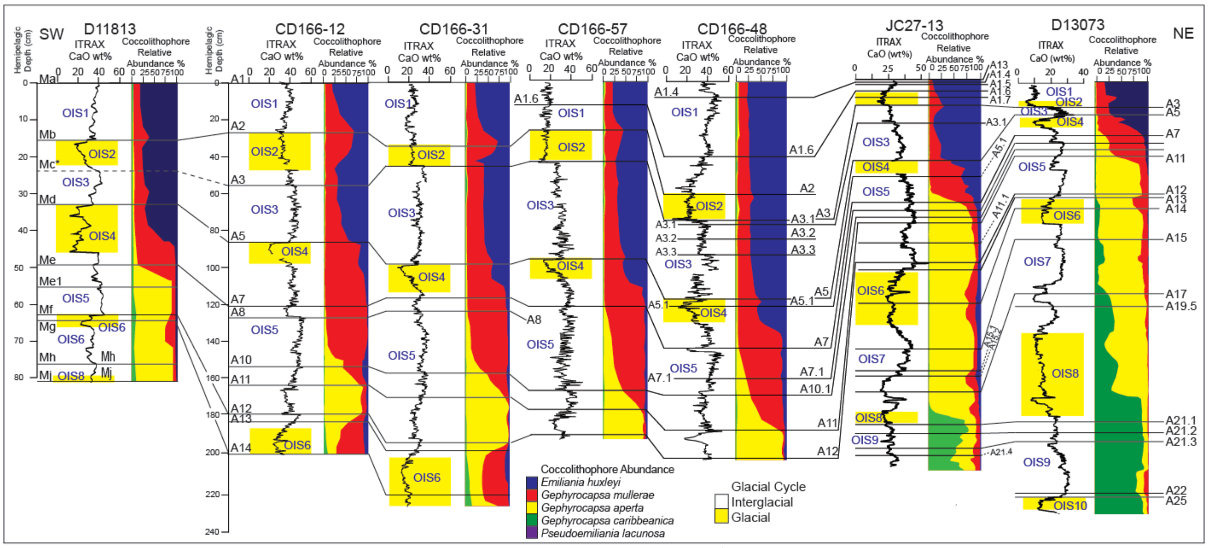
SW
NE
D11813
CD166-12
CD166-31
CD166-57
CD166-48
JC27-13
D13073
Hemipelagic Depth (cm)
ITRAX CaO wt%
Coccolithophore Relative Abundance %
Coccolithophore Abundance
Emiliania huxleyi
Gephyrocapsa mullerae
Gephyrocapsa aperta
Gephyrocapsa caribbeanica
Pseudoemiliania lacunosa
Glacial Cycle
Interglacial
Glacial

Figure 3

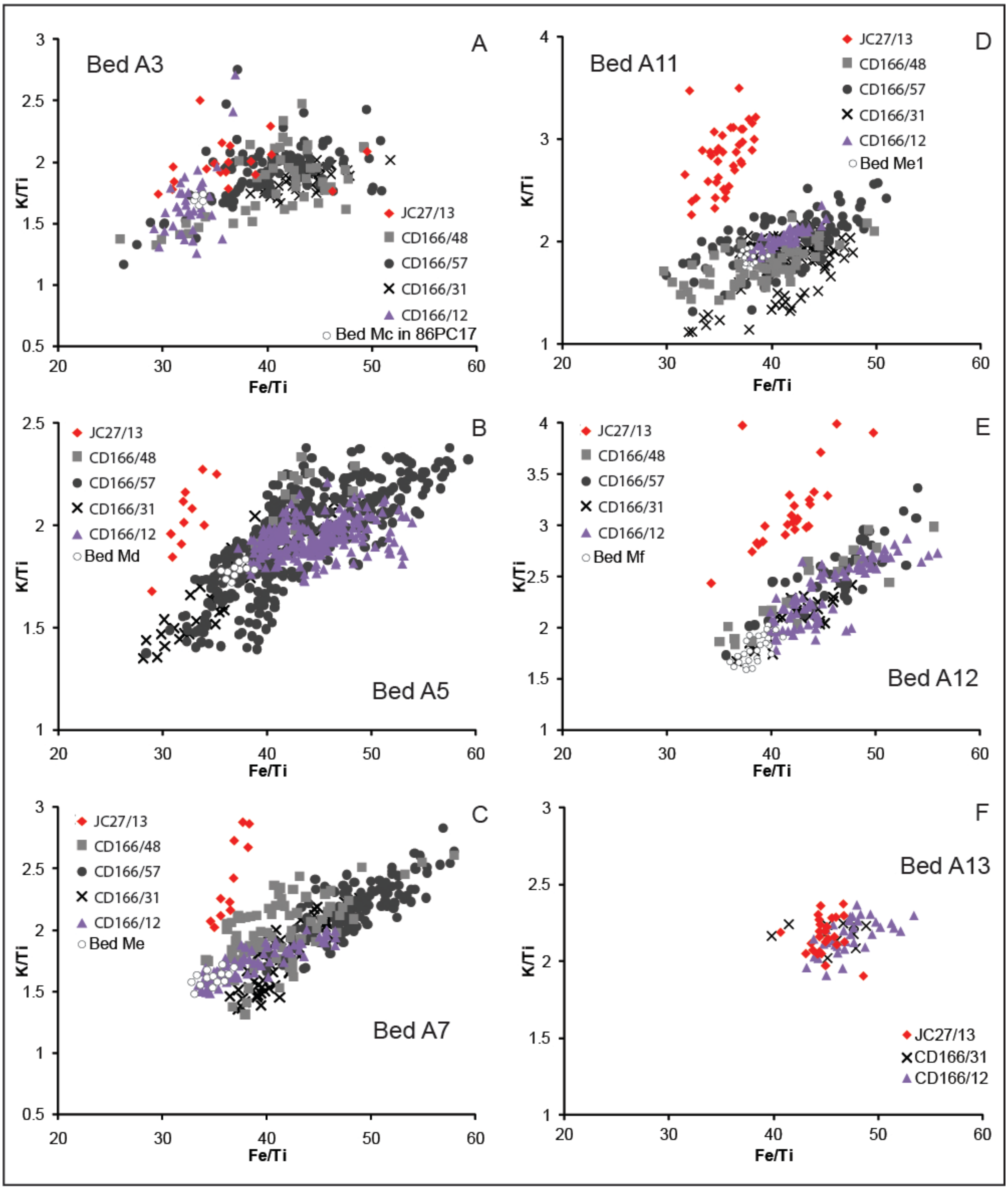
A
Bed A3
K/Ti
Fe/Ti
JC27/13
CD166/48
CD166/57
CD166/31
CD166/12
Bed Mc in 86PC17
D
Bed A11
K/Ti
Fe/Ti
JC27/13
CD166/48
CD166/57
CD166/31
CD166/12
Bed Me1
B
Bed A5
K/Ti
Fe/Ti
JC27/13
CD166/48
CD166/57
CD166/31
CD166/12
Bed Md
E
Bed A12
K/Ti
Fe/Ti
JC27/13
CD166/48
CD166/57
CD166/31
CD166/12
Bed Mf
C
Bed A7
K/Ti
Fe/Ti
JC27/13
CD166/48
CD166/57
CD166/31
CD166/12
Bed Me
F
Bed A13
K/Ti
Fe/Ti
JC27/13
CD166/31
CD166/12

Figure 4

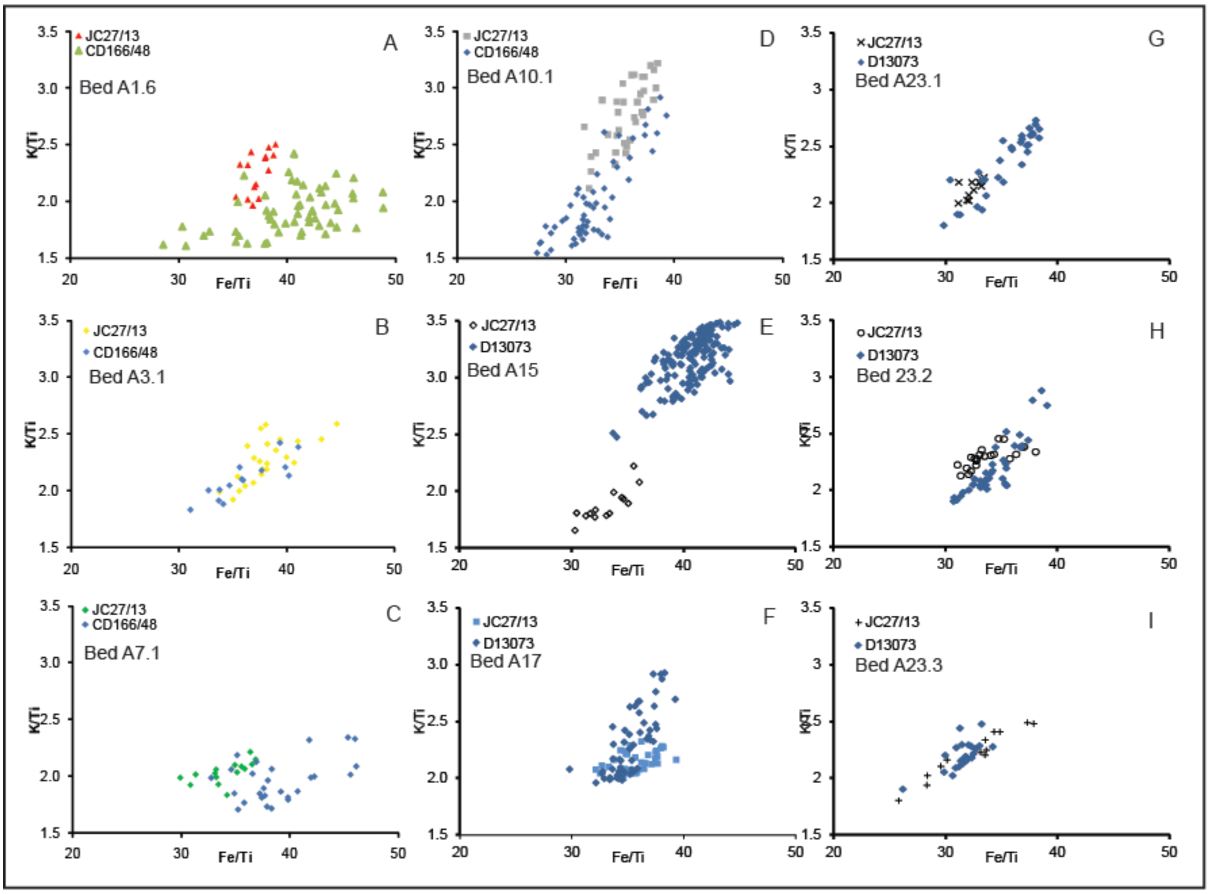
JC27/13
CD166/48
Bed A1.6
A
D13073
Bed A10.1
D
Bed A23.1
G
Bed A3.1
B
Bed A15
E
Bed 23.2
H
Bed A7.1
C
Bed A17
F
Bed A23.3
I
K/Ti
Fe/Ti

Figure 5

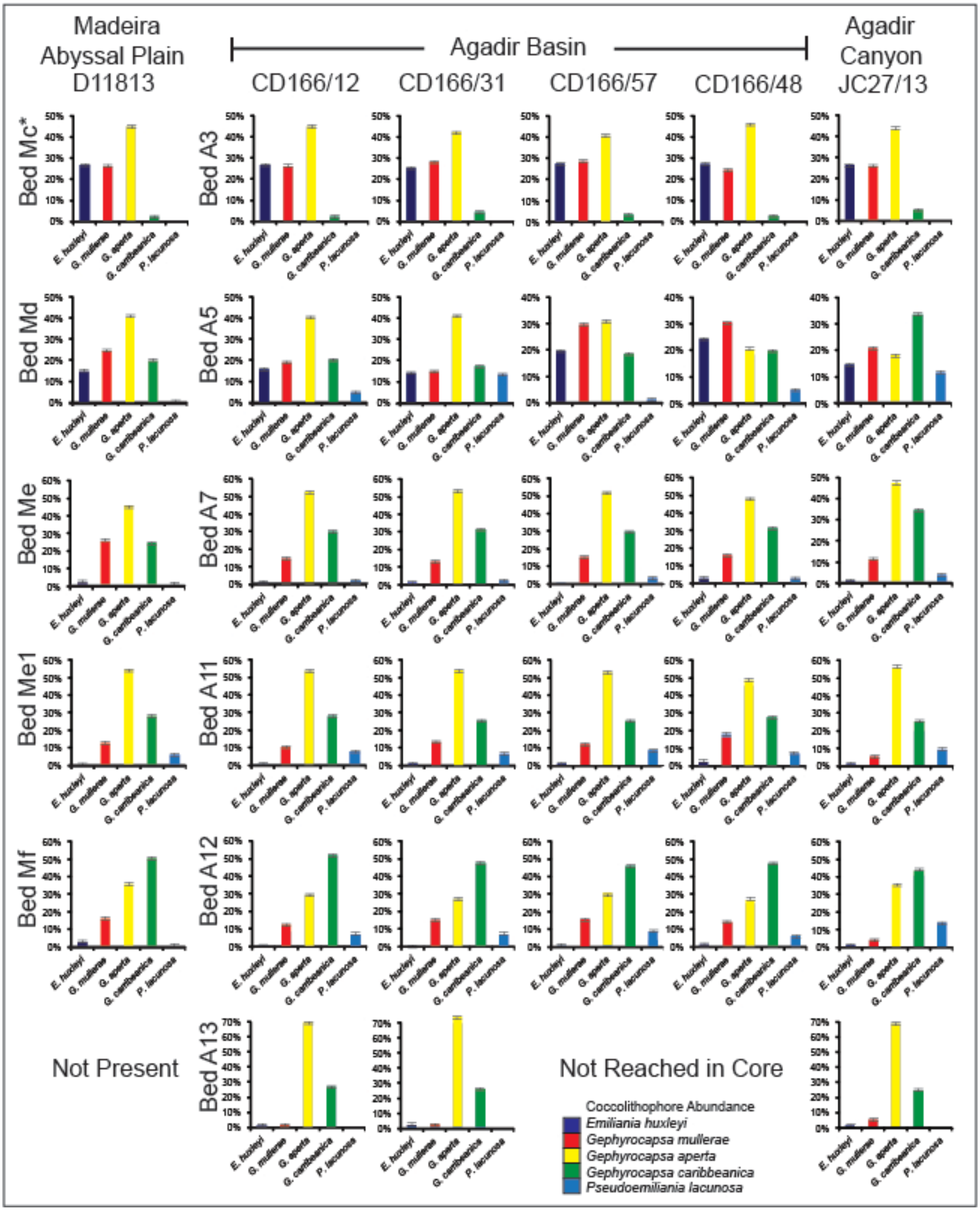
Madeira Abyssal Plain D11813
Agadir Basin
CD166/12
CD166/31
CD166/57
CD166/48
Agadir Canyon JC27/13
Bed Mc*
Bed A3
Bed Md
Bed A5
Bed Me
Bed A7
Bed Me1
Bed A11
Bed Mf
Bed A12
Bed A13
Not Present
Not Reached in Core
E. huxleyi
G. mullerae
G. aperta
G. caribbeanica
P. lacunosa
Coccolithophore Abundance
Emiliania huxleyi
Gephyrocapsa mullerae
Gephyrocapsa aperta
Gephyrocapsa caribbeanica
Pseudoemiliania lacunosa

Figure 6

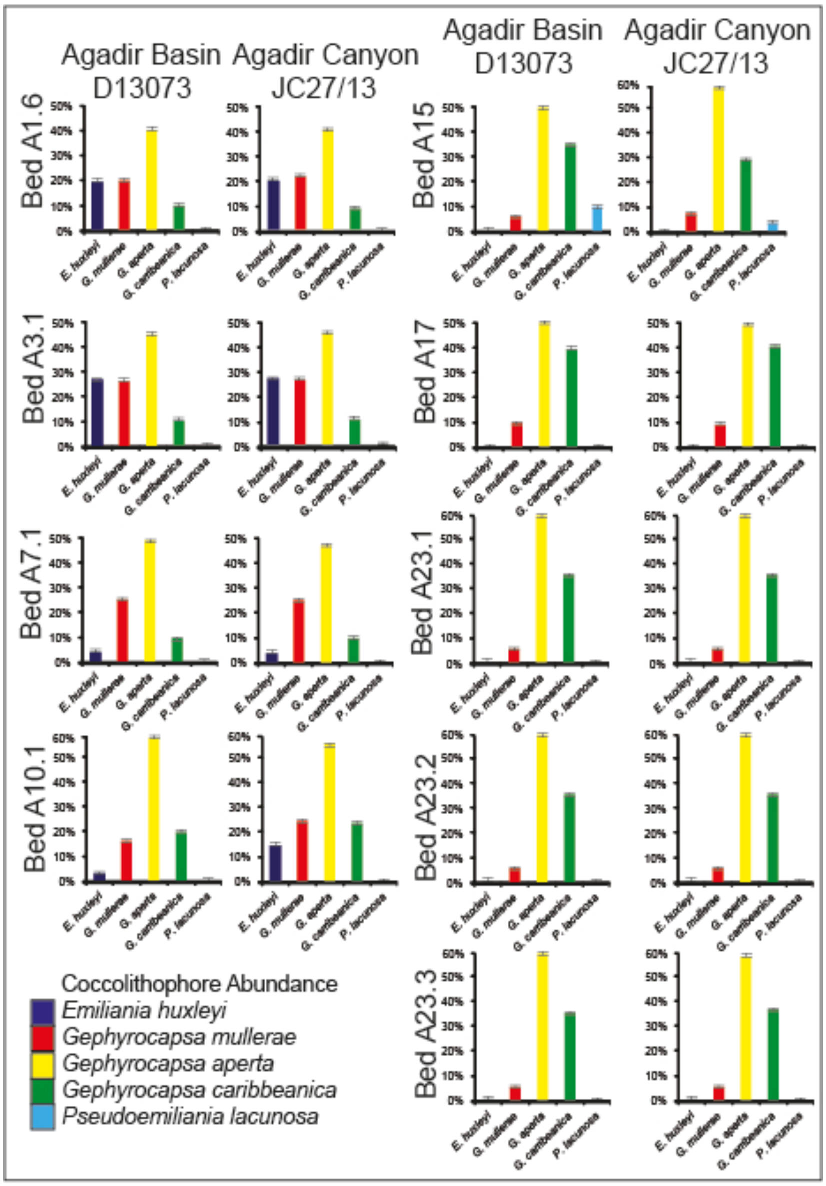
Agadir Basin
D13073
Agadir Canyon
JC27/13
Bed A1.6
Bed A3.1
Bed A7.1
Bed A10.1
Bed A15
Bed A17
Bed A23.1
Bed A23.2
Bed A23.3
E. huxleyi
G. mullerae
G. aperta
G. caribbeanica
P. lacunosa
Coccolithophore Abundance
Emiliania huxleyi
Gephyrocapsa mullerae
Gephyrocapsa aperta
Gephyrocapsa caribbeanica
Pseudoemiliania lacunosa

Figure 7

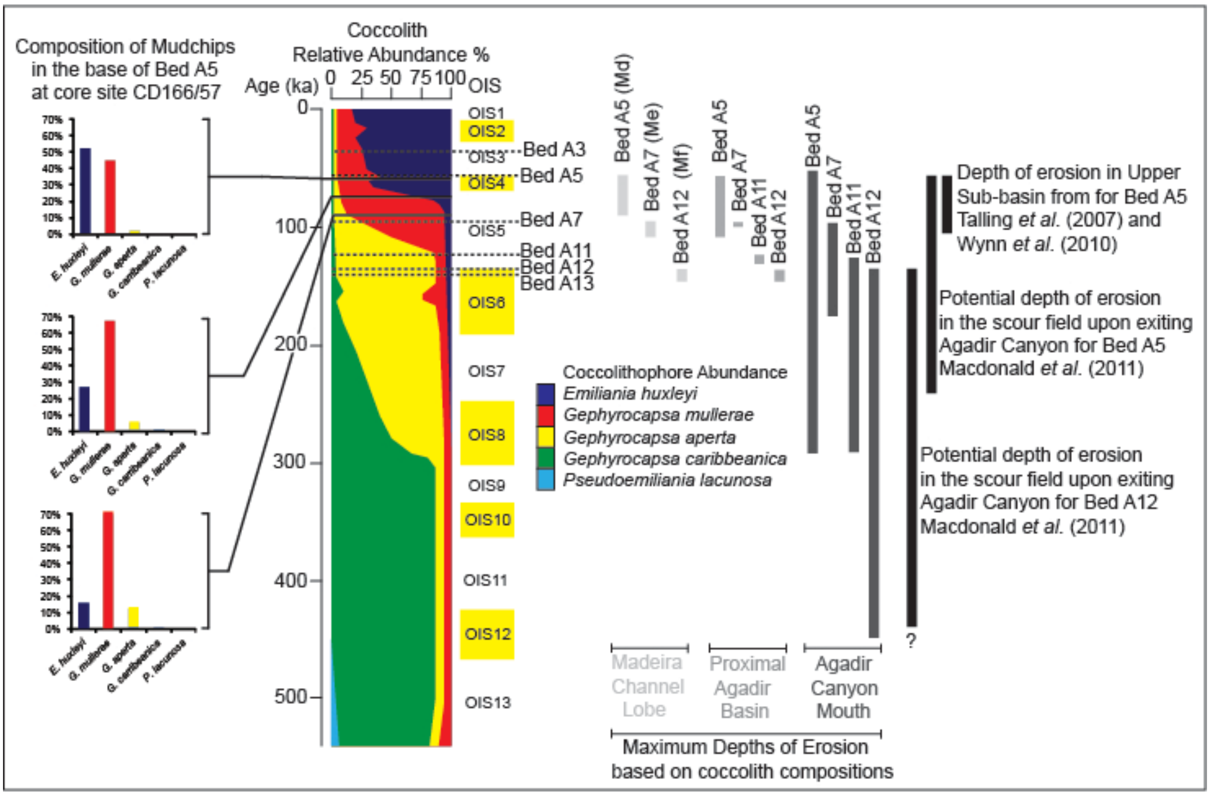
Composition of Mudchips in the base of Bed A5 at core site CD166/57
Coccolith Relative Abundance %
Age (ka)
0 25 50 75 100
OIS
OIS1
OIS2
OIS3
OIS4
OIS5
OIS6
OIS7
OIS8
OIS9
OIS10
OIS11
OIS12
OIS13
Bed A3
Bed A5
Bed A7
Bed A11
Bed A12
Bed A13
Coccolithophore Abundance
Emiliania huxleyi
Gephyrocapsa mullerae
Gephyrocapsa aperta
Gephyrocapsa caribbeanica
Pseudoemiliania lacunosa
Bed A5 (Md)
Bed A7 (Me)
Bed A12 (Mf)
Madeira Channel Lobe
Proximal Agadir Basin
Agadir Canyon Mouth
Maximum Depths of Erosion based on coccolith compositions
Depth of erosion in Upper Sub-basin from for Bed A5 Talling et al. (2007) and Wynn et al. (2010)
Potential depth of erosion in the scour field upon exiting Agadir Canyon for Bed A5 Macdonald et al. (2011)
Potential depth of erosion in the scour field upon exiting Agadir Canyon for Bed A12 Macdonald et al. (2011)

Figure 8

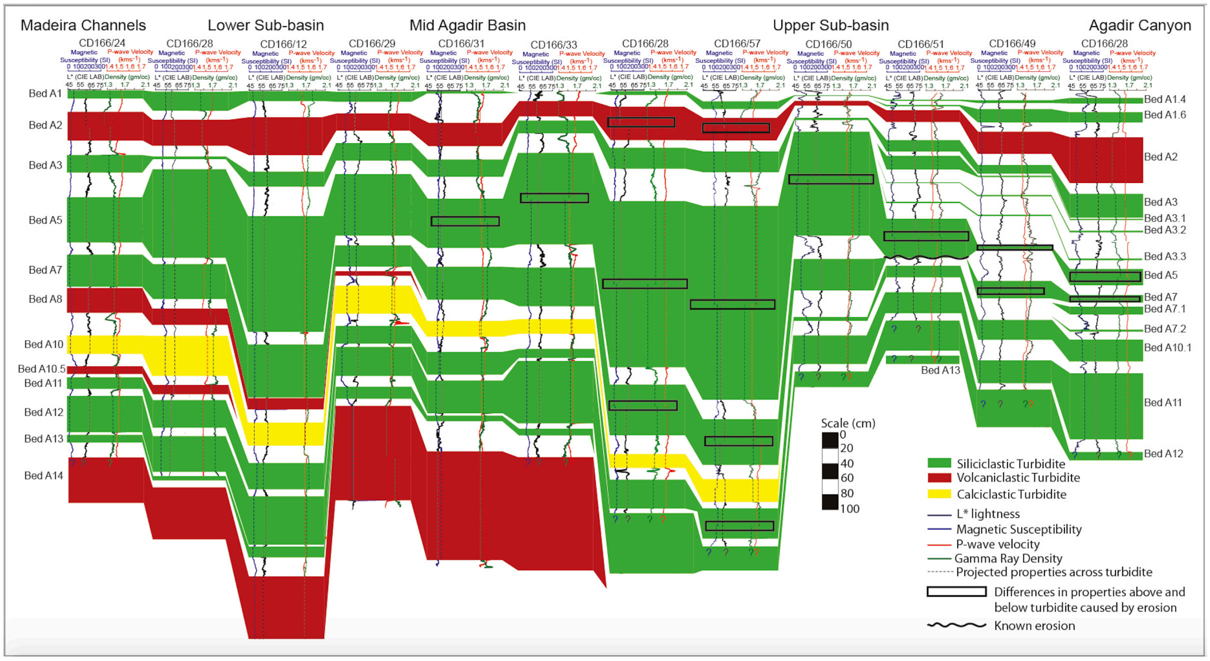

Madeira Channels
Lower Sub-basin
Mid Agadir Basin
Upper Sub-basin
Agadir Canyon
CD166/24
CD166/28
CD166/12
CD166/29
CD166/31
CD166/33
CD166/28
CD166/57
CD166/50
CD166/51
CD166/49
CD166/28
Magnetic Susceptibility (SI)
P-wave Velocity (kms⁻¹)
L* (CIE LAB)
Density (gm/cc)
Bed A1
Bed A2
Bed A3
Bed A5
Bed A7
Bed A8
Bed A10
Bed A10.5
Bed A11
Bed A12
Bed A13
Bed A14
Bed A1.4
Bed A1.6
Bed A2
Bed A3
Bed A3.1
Bed A3.2
Bed A3.3
Bed A5
Bed A7
Bed A7.1
Bed A7.2
Bed A10.1
Bed A11
Bed A12
Bed A13
Scale (cm)
0
20
40
60
80
100
Siliciclastic Turbidite
Volcaniclastic Turbidite
Calciclastic Turbidite
L* lightness
Magnetic Susceptibility
P-wave velocity
Gamma Ray Density
Projected properties across turbidite
Differences in properties above and below turbidite caused by erosion
Known erosion

Figure 9

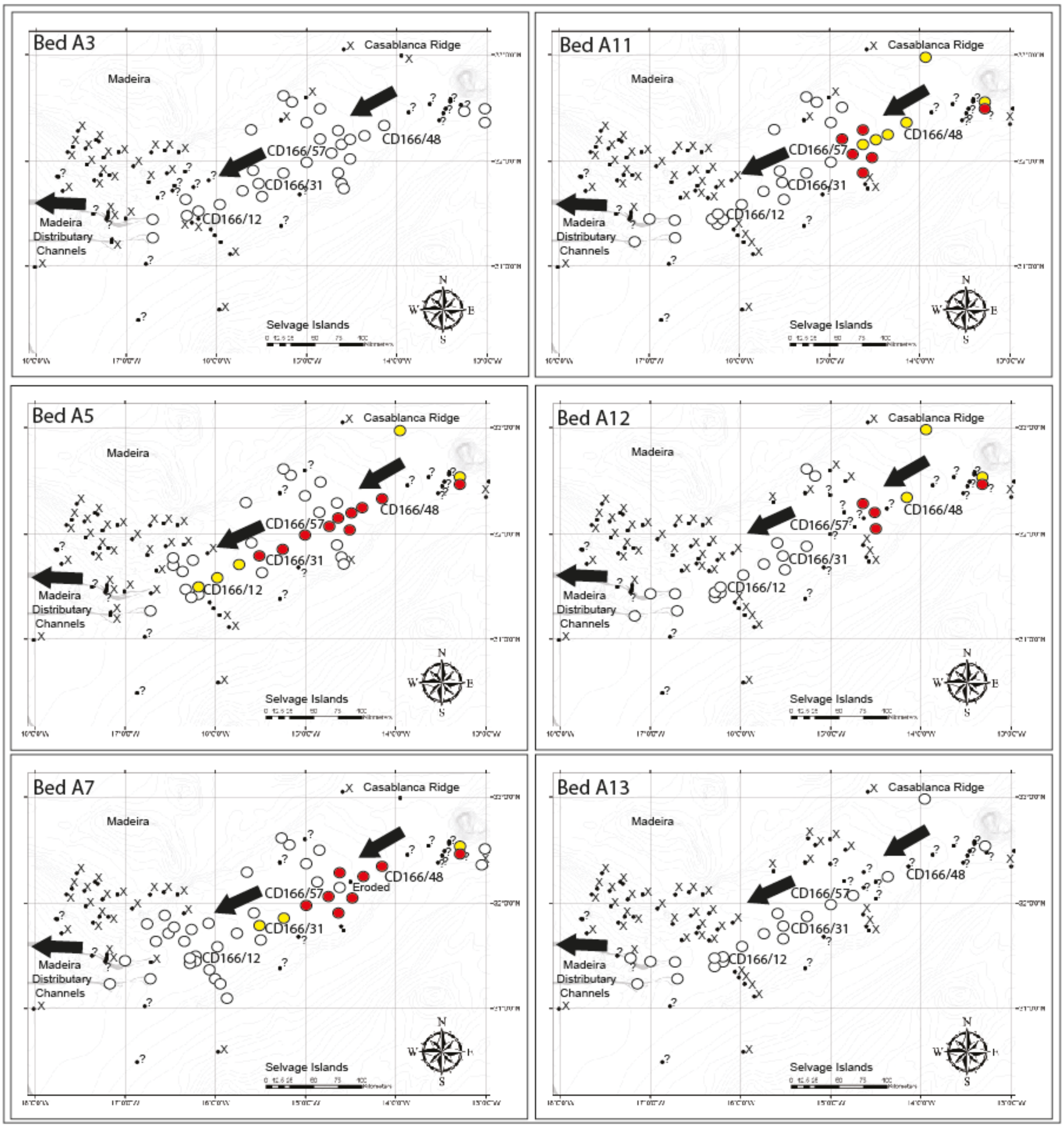
Bed A3
Casablanca Ridge
Madeira
CD166/48
CD166/57
CD166/31
CD166/12
Madeira Distributary Channels
Selvage Islands
Bed A11
Casablanca Ridge
Madeira
CD166/48
CD166/57
CD166/31
CD166/12
Madeira Distributary Channels
Selvage Islands
Bed A5
Casablanca Ridge
Madeira
CD166/48
CD166/57
CD166/31
CD166/12
Madeira Distributary Channels
Selvage Islands
Bed A12
Casablanca Ridge
Madeira
CD166/48
CD166/57
CD166/31
CD166/12
Madeira Distributary Channels
Selvage Islands
Bed A7
Casablanca Ridge
Madeira
CD166/48
Eroded
CD166/57
CD166/31
CD166/12
Madeira Distributary Channels
Selvage Islands
Bed A13
Casablanca Ridge
Madeira
CD166/48
CD166/57
CD166/31
CD166/12
Madeira Distributary Channels
Selvage Islands

Figure 10

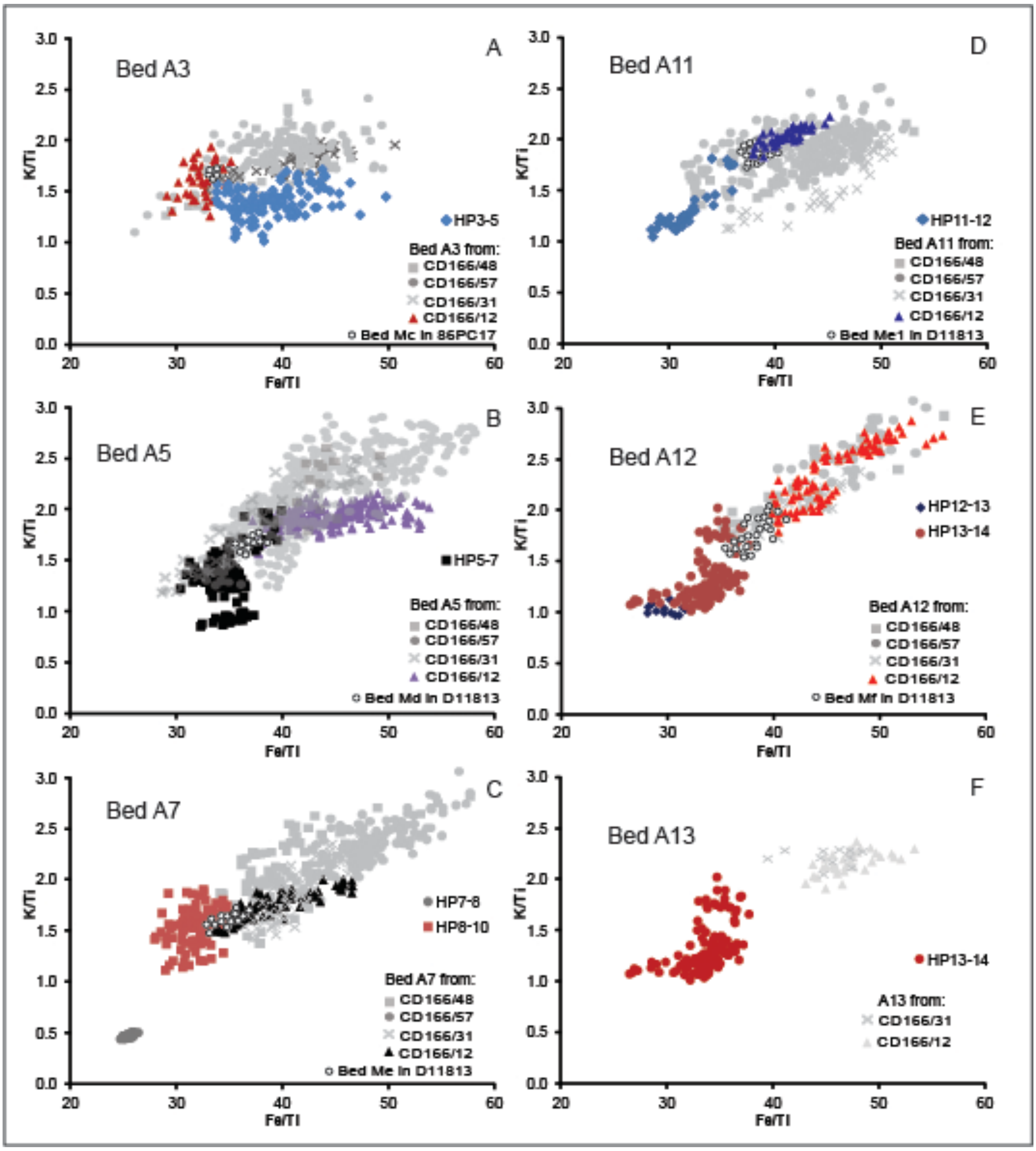
Bed A3
A
HP3-5
Bed A3 from:
CD166/48
CD166/57
CD166/31
CD166/12
Bed Mc in 86PC17
Bed A11
D
HP11-12
Bed A11 from:
CD166/48
CD166/57
CD166/31
CD166/12
Bed Me1 in D11813
Bed A5
B
HP5-7
Bed A5 from:
CD166/48
CD166/57
CD166/31
CD166/12
Bed Md in D11813
Bed A12
E
HP12-13
HP13-14
Bed A12 from:
CD166/48
CD166/57
CD166/31
CD166/12
Bed Mf in D11813
Bed A7
C
HP7-8
HP8-10
Bed A7 from:
CD166/48
CD166/57
CD166/31
CD166/12
Bed Me in D11813
Bed A13
F
HP13-14
A13 from:
CD166/31
CD166/12
K/Ti
Fe/Ti

Figure 11